



Review

Recent Advances of First d-Block Metal-Based Perovskite Oxide Electrocatalysts for Alkaline Water Splitting

Jian Wang ¹, Subin Choi ¹, Juwon Kim ¹, Suk Won Cha ² and Jongwoo Lim ^{1,*}

¹ Department of Chemistry, Seoul National University, Seoul 08826, Korea; jwangbx@snu.ac.kr (J.W.); sbchoi01@snu.ac.kr (S.C.); prime4020@snu.ac.kr (J.K.)

² Department of Mechanical and Aerospace Engineering, Seoul National University, 1 Gwanak-ro, Gwanak-gu, Seoul 08826, Korea; swcha@snu.ac.kr

* Correspondence: jwlim@snu.ac.kr

Received: 30 June 2020; Accepted: 8 July 2020; Published: 9 July 2020



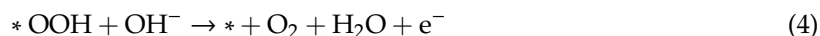
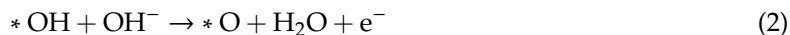
Abstract: First d-block metal-based perovskite oxides (FDMPOs) have garnered significant attention in research for their utilization in the water oxidation reaction due to their low cost, earth abundance, and promising activities. Recently, FDMPOs are being applied in electrocatalysis for the hydrogen evolution reaction (HER) and overall water splitting reaction. Numerous promising FDMPO-based water splitting electrocatalysts have been reported, along with new catalytic mechanisms. Therefore, an in-time summary of the current progress of FDMPO-based water splitting electrocatalysts is now considered imperative. However, few reviews have focused on this particular subject thus far. In this contribution, we review the most recent advances (mainly within the years 2014–2020) of FDMPO electrocatalysts for alkaline water splitting, which is widely considered to be the most promising next-generation technology for future large-scale hydrogen production. This review begins with an introduction describing the fundamentals of alkaline water electrolysis and perovskite oxides. We then carefully elaborate on the various design strategies used for the preparation of FDMPO electrocatalysts applied in the alkaline water splitting reaction, including defecting engineering, strain tuning, nanostructuring, and hybridization. Finally, we discuss the current advances of various FDMPO-based water splitting electrocatalysts, including those based on Co, Ni, Fe, Mn, and other first d-block metal-based catalysts. By conveying various methods, developments, perspectives, and challenges, this review will contribute toward the understanding and development of FDMPO electrocatalysts for alkaline water splitting.

Keywords: perovskite oxides; first d-block; electrocatalyst; alkaline water splitting

1. Introduction

Water electrolysis is garnering extensive interest for the clean production of hydrogen, notably with the advantages of high efficiency, abundant sources, mild environmental impact, etc. In addition, by storing electricity in the form of chemical energy (i.e., hydrogen), water electrolysis helps to mitigate the intermittent issue of renewable energies (e.g., wind, solar). Water electrolysis is a process that decomposes water into oxygen and hydrogen using external electrical energy; it is composed of two half-reactions; namely, the anodic oxygen evolution reaction (OER) and cathodic hydrogen evolution reaction (HER). Both the OER and HER are multi-electron processes involving several reactive intermediates, such as H, OH, and O. In alkaline media, the OER generally proceeds via the following pathway on the active sites (*) [1]:



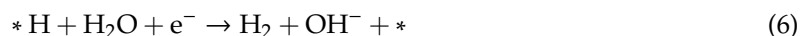


For the HER, it takes place via the following mechanism [2]:

Volmer step:



Heyrovsky step:

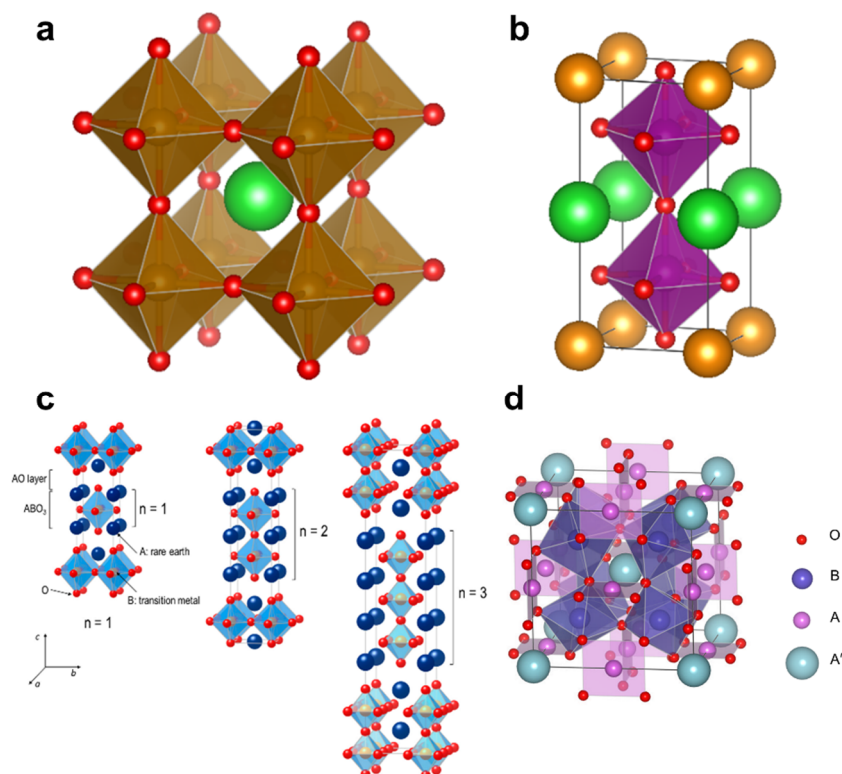


Or Tafel step:



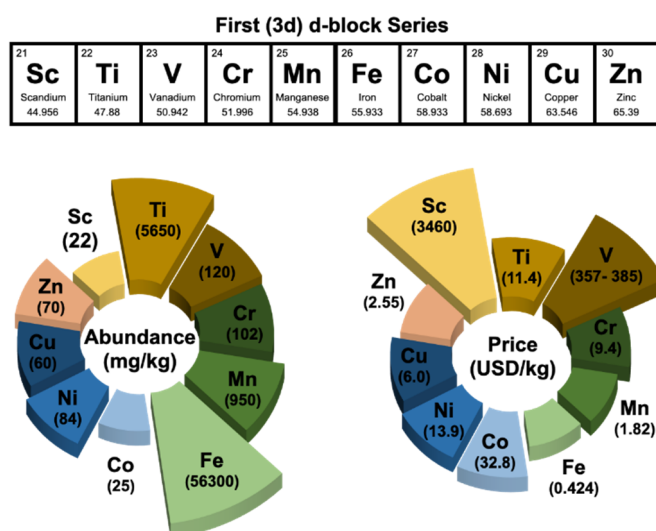
The sluggish kinetics observed for the OER and HER are among the most serious bottlenecks preventing the mass-adoption of water electrolyzers [3]. Alkaline water electrolysis renders it possible to utilize non-precious metal-based electrocatalysts, and is thereby widely considered to be the most promising method for large-scale application of water electrolyzers for hydrogen production [4].

Among the various non-precious electrocatalysts reported thus far [5,6], perovskite-type oxides have garnered much attention due to their low cost, earth abundance, and promising activities [7–9]. Primitive perovskite oxides have the general formula ABO_3 , where the A-site cation is usually an alkaline/rare-earth metal, while the B-site is occupied by a transition metal surrounded by six oxygen atoms. In addition to primitive perovskite oxides (ABO_3), double-(A-site ordered ($\text{A}_2\text{BB}'\text{O}_6$) and B-site ordered ($\text{A}_2\text{BB}'\text{O}_6$)), Ruddlesden–Popper ($\text{A}_{n+1}\text{B}_n\text{O}_{3n+1}$), and quadruple ($\text{AA}'_3\text{B}_4\text{O}_{12}$) types have also been studied for water electrolysis (Scheme 1) [10–12]. The structure of perovskite oxides is flexible and can accommodate different levels of oxygen vacancies and various dopants, allowing their composition to be easily modified. As a result, the catalytic performance of perovskite oxides toward water electrolysis can be easily tuned and optimized.



Scheme 1. Illustration of the various structures of perovskite oxides. (a) Primitive perovskite with an ideal cubic structure; (b) A-site ordered double perovskite oxide with a tetragonal structure; and (c) layered perovskite with a Ruddlesden–Popper structure ($A_{n+1}B_nO_{3n+1}$, $n = 1, 2$, and 3); reproduced with permission [13] Copyright (2017), Publisher: MDPI; (d) Quadruple-type perovskite ($AA'B_4O_{12}$).

For perovskite oxides, the adsorption energies of the reaction intermediates determine their catalytic activity to a large extent, which is typically influenced by the electronic configuration on the catalyst surface [14]. First d-block metal-based (e.g., Co, Ni, Fe, Mn, Cu, Cr, V, and Ti) perovskite oxides can utilize the unique characteristics of 3d valence electrons and have attracted much attention for water electrolysis [15]. In addition, first d-block metals are relatively abundant and cheap; their earth abundance and current price are shown in Scheme 2. Consequently, first d-block metal-based perovskite oxides (FDMPOs) have been extensively investigated for use in the water oxidation reaction [16]. Recently, extending the application of perovskite oxides toward the HER [17,18] and overall water splitting reaction [8,19] has also become popular. An in-time summary of the strategies used to rationally design perovskite oxides and their current progress will be beneficial for their further development. Although there are several excellent reviews on perovskite electrocatalysts [9,20,21], the efforts of reviews on FDMPOs used in water electrolysis are few, which motivates us to mitigate this gap. We aim to contribute to the development of perovskite oxide-based electrocatalysts that are used for the alkaline water splitting reaction by presenting design strategies and current advances.



Scheme 2. Earth abundance of first d-block transition metals (mg/kg) and their current price (USD/kg) [22].

2. Design Strategies

In general, there are two strategies used to design superior perovskite oxide-based water splitting electrocatalysts. One is to improve the intrinsic activity, while the other is to enhance the number of active sites. The specific methods used to achieve these strategies include defect engineering, strain tuning, nanostructuring, and hybridization, which are summarized below.

2.1. Defect Engineering

Defect engineering is commonly used to modify the electronic structure and enhance the intrinsic activity of perovskite oxide catalysts [23]. The strategies of engineering perovskite defects include the introduction of dopants [24–27] and modulating their deficiencies [28,29]. Specifically, dopants can be introduced into the A- [30,31], B- [32,33] and oxygen-sites [34,35]. One of the well-known examples is Fe-doping in the B-site of cobalt-based perovskite oxides, which has been

demonstrated to significantly boost the OER activity [36]. In order to clarify the mechanism behind the positive role of Fe-doping, operando Co K-edge X-ray absorption fine structure (XAFS) spectra were collected for $\text{Ba}_{0.5}\text{Sr}_{0.5}\text{Co}_{0.8}\text{Fe}_{0.2}\text{O}_{3-\delta}$ (BSCF) and $\text{Ba}_{0.5}\text{Sr}_{0.5}\text{CoO}_{3-\delta}$ (BSC) during the OER. From the Fourier-transformed extended X-ray absorption fine structure (FT-EXAFS) spectra shown in Figure 1a, a more noticeable development of the Co-Co coordination peak (represented by the dashed line) was observed on BSCF when compared to that on BSC, indicating that the formation of an increased number of $\text{CoO}(\text{OH})$ active species was responsible for the higher activity [37]. A-site dopants usually play an important role in influencing the catalytic activity of perovskite oxides by modifying the electronic configuration of the B-site cations. For example, partial substitution of La with Sr in LaCoO_3 has also been reported to optimize the oxygen adsorption energy of cobalt and boost the OER activity [38]. In addition to OER catalysis, doping in perovskite oxides has also been investigated in the HER. If the perovskite surface binds H too weakly, the overall HER rate is limited by the adsorption (Volmer) step. On the other hand, an excessively strong binding with H renders the desorption step difficult and limits the Heyrovsky/Tafel step rate. As a result, the binding of H on the perovskite oxide surface (H_{ad}) is critical for HER activity. In a recent study, anionic F-doping was introduced into $\text{La}_{0.5}\text{Ba}_{0.25}\text{Sr}_{0.25}\text{CoO}_{3-\delta}$ (LBSC) to optimize the H_{ad} and boost the HER activity. In comparison to pristine LBSC (-0.634 eV), $\text{La}_{0.5}\text{Ba}_{0.25}\text{Sr}_{0.25}\text{CoO}_{2.9-\delta}\text{F}_{0.1}$ (LBSCF) exhibited a more favorable ΔG_{H^*} value (-0.279 eV), which was closer to zero (not too strong or weak binding) and contributed to the higher HER activity [39].

Similar to the doping strategy, modulating the compositions of the deficiencies in the perovskite A-sites [40,41] and oxygen sites [42] is also a promising strategy for tuning the catalytic properties. Oxygen vacancies are generally considered beneficial for the intake of hydroxyl groups and OER activity [42,43]. However, recent works have demonstrated that there is an optimal concentration of oxygen vacancies for catalyzing the OER [44,45]. By varying the oxygen gas partial pressure, the oxygen vacancy concentration inside NdNiO_3 can be easily tuned [44]. By comparison, the OER activity of NdNiO_3 displayed a volcano-type relationship with the oxygen partial pressure, and the highest OER activity was achieved at a moderate oxygen partial pressure (i.e., 10 Pa, Figure 1c), in which the oxygen vacancy concentration and the Ni valence are balanced [44]. In another work, a large increase in the number of oxygen vacancies was found to be detrimental to the intrinsic OER activity of $\text{PrBaCo}_2\text{O}_{6-\delta}$ [45]. The increased number of oxygen vacancies tend to align orderly in $\text{PrO}_{1-\delta}$, which not only lowered the cobalt valence state, but also induced the cobalt transition from a high-spin to low-spin state, resulting in significant deceleration of the OER kinetics [45]. The roles of the oxygen vacancies are assumed to be multi-sided and require further investigation. Since the highly oxidizing environments during the OER may oxidize the lattice oxygen [46], the stability of highly oxygen-deficient perovskite oxides is also worth studying.

2.2. Strain Tuning

In addition to resorting to defects, engineering the strain can also modify the electronic structure of perovskite oxides and further tune the intrinsic activity [47,48]. Epitaxial growth is one of the standard methods for building strain in the lattice of perovskites. Strain is induced due to the mismatch when two planes with different lattice parameters are firmly connected to one another. By carefully choosing the substrate with a wide range of lattice spacings, the lattice mismatch can be tuned, generating tensile or compressive strain. The strain propagates into the internal solid film and gradually relaxes. Strain plays a role in modifying the catalytic performance of perovskites by changing the TM-O bond length and distorting the octahedra [49]. By controlling the lattice orientation of LaCoO_3 (LCO) epitaxial films, Xie and coworkers prepared a series of strained LaCoO_3 films with different degrees of distortion in the CoO_6 octahedron. They found that the strain-induced distortion causes a cobalt spin-state transition from the low spin state ($t_{2g}^6e_g^0$) to an intermediate spin state ($t_{2g}^5e_g^1$) in LCO(100) film, as shown in Figure 2(a1). This optimized e_g orbital filling lowered the OER adsorption energy of LCO(100) (Figure 2(a2)), contributing to the excellent OER activity [50].

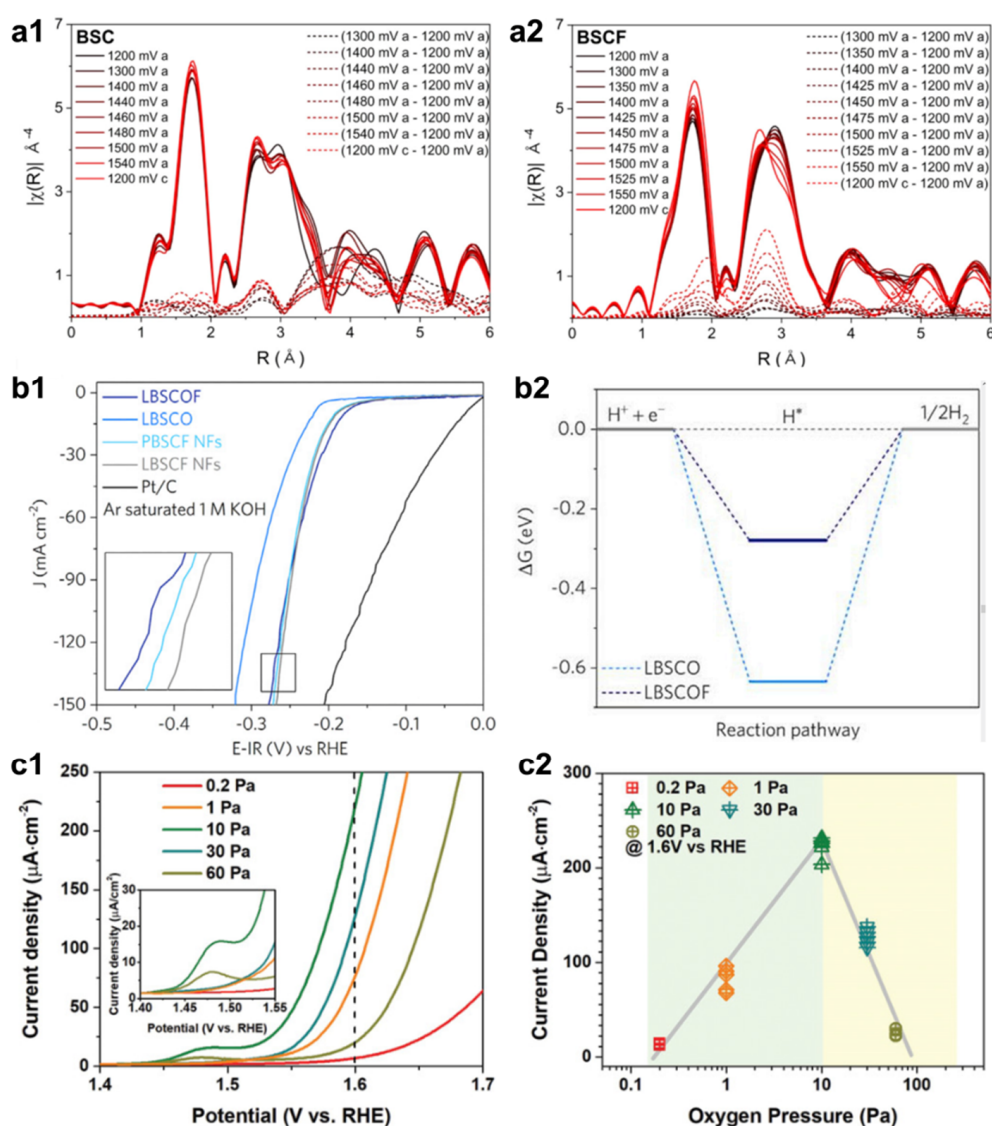


Figure 1. (a) Cationic Fe-doping boosts the in-situ formation of (oxy)hydroxide on the surface of BSCF. Fourier transformed (FT) k^3 -weighted Co K-edge EXAFS (extended X-ray absorption fine structure) spectra obtained for (a1) BSC and (a2) BSCF during the OER (oxygen evolution reaction); reproduced with permission [37] Copyright (2019), American Chemical Society. (b) Anionic F-doping boosts the HER (hydrogen evolution reaction) activity of $\text{La}_{0.5}\text{Ba}_{0.25}\text{Sr}_{0.25}\text{CoO}_{3-\delta}$. A comparison of the (b1) HER polarization curve and (b2) HER Gibbs free energy; reproduced with permission [39] Copyright (2018), Elsevier. (c) Oxygen partial pressure tunes the oxygen vacancies in NdNiO_3 and enhances the OER activity: (c1) OER polarization curve obtained for NdNiO_3 at different oxygen pressures and (c2) volcano plot obtained for the OER current density as a function of the oxygen pressure; reproduced with permission [44] Copyright (2019), John Wiley and Sons.

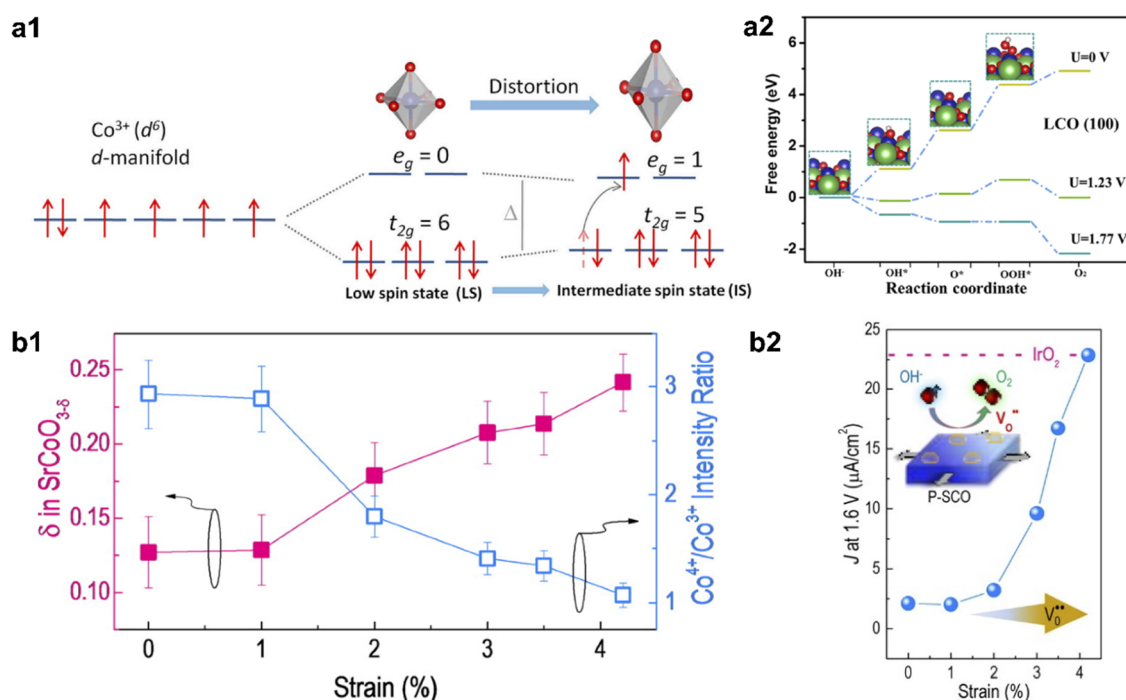


Figure 2. (a) Strain-induced distortion of the CoO_6 octahedron in LaCoO_3 optimizes the e_g orbital filling and OER activity: (a1) A comparison of the spin states and (a2) the OER free-energy diagrams obtained for the LCO (100) film depending on the reaction coordinates; reproduced with permission [50] Copyright (2017), Elsevier. (b) Strain-induced tuning of the oxygen vacancies boosts the OER activity: (b1) the dependence of the number of oxygen vacancies (δ) and $\text{Co}^{4+}/\text{Co}^{3+}$ ratio in $\text{SrCoO}_{3-\delta}$ perovskite on the tensile strain, and (b2) the OER current density observed at 1.6 V vs. reversible hydrogen electrode (RHE) as a function of strain; reproduced with permission [47] Copyright (2016), American Chemical Society.

Epitaxial strain is also a powerful tool used to manipulate the oxygen vacancy concentration inside perovskites beyond adjusting the electronic configurations [51]. Lee and coworkers demonstrated that tensile strain can assist $\text{SrCoO}_{3-\delta}$ to maintain a certain number of oxygen vacancies during the OER, in contrast to the pristine $\text{SrCoO}_{3-\delta}$ which was almost fully oxidized and contained few oxygen vacancies (Figure 2(b1)). Due to the well-maintained oxygen vacancies, strained $\text{SrCoO}_{3-\delta}$ achieved an excellent OER activity, which was comparable to that of IrO_2 (Figure 2(b2)) [47].

Epitaxial growth-prepared strained thin films serve as an ideal platform for the fundamental study of perovskite oxides. However, investigations on the mechanisms of the changes observed in the reactivity of epitaxially-strained films should be carefully undertaken due to the convoluted effects of the defects and the film thickness-dependent strain states [52]. In addition, it is challenging to apply solid thin films for practical water electrolysis due to the lack of porosity and the high preparation cost. The introduction of strains into nanostructured perovskite particles is suggested for future studies to prepare highly-active electrocatalysts. Furthermore, the stability of strains during OER and HER is also worth investigating.

2.3. Nanostructuring

Thanks to the development of oxide-based nanomaterial synthesis methodologies, various nanostructures have been fabricated for perovskite oxides, such as nanoparticles [53,54], nanofibers [55,56], nanorods [57,58], nanotubes [59], and nanosheets [60]. A wide range of synthetic approaches have been reported, including wet chemistry methods (e.g., sol-gel, hydrothermal), deposition (e.g., physical laser deposition (PLD), chemical vapor deposition (CVD), and electrodeposition), electrospinning, exsolution, infiltration, and template-assisted synthesis. The rationale behind the nanostructuring

strategy is to increase the surface area and expose more active sites [61,62]. Shao and co-workers fabricated $\text{SrNb}_{0.1}\text{Co}_{0.7}\text{Fe}_{0.2}\text{O}_{3-\delta}$ nanorods (SNCF-NR, Figure 3(a1)) using an electrospinning technique, which display promising bifunctional OER and HER activity [58]. The overall water splitting activity of SNCF-NR examined using a homemade water electrolyzer was observed to be superior to that achieved with a commercial catalyst pair (Pt/C–IrO₂) at a high current density (Figure 3(a2)). In addition to exposing more surface sites to facilitate access to the electrolyte [63], the down-sized structure altered the electronic configuration of the perovskite oxide [54]. The e_g orbital filling of LaCoO_3 perovskite oxide was found to be highly dependent on the particle size (Figure 3(b1)). Upon reducing the LaCoO_3 particle sizes from 200 to 60 nm, the corresponding e_g orbital filling of cobalt increased gradually from 1.1 to 1.27, as shown in Figure 3(b2). This change was attributed to the spin-state transition from the low-spin to high-spin states observed for the cobalt ions on the nanoparticle surface. LaCoO_3 with a particle size of 80 nm exhibited an optimal e_g orbital filling of 1.2 and achieved the best OER activity [54].

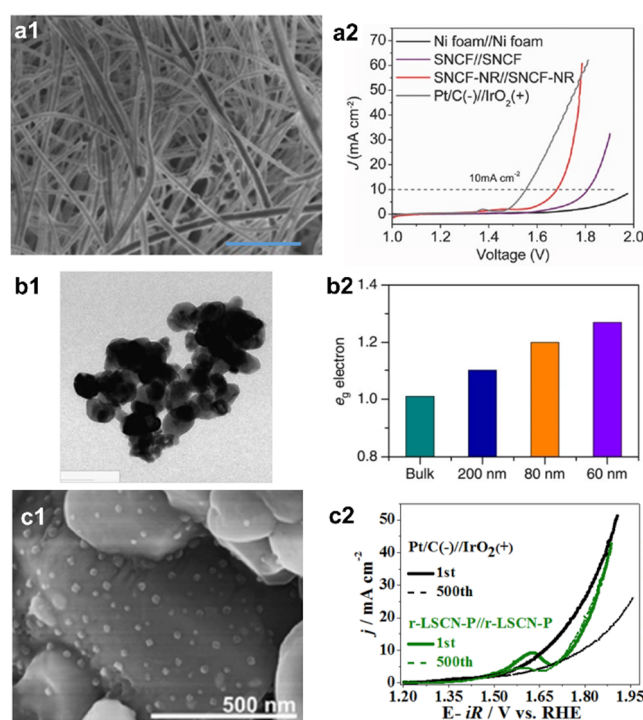


Figure 3. (a) $\text{SrNb}_{0.1}\text{Co}_{0.7}\text{Fe}_{0.2}\text{O}_{3-\delta}$ nanorods used as a bifunctional catalyst for the overall water splitting reaction: (a1) TEM (transmission electron microscope) image and (a2) water splitting polarization curve; reproduced with permission [58] Copyright (2017), John Wiley and Sons. (b) Nanoparticles optimize the e_g orbital occupancy and enhance the OER activity of LaCoO_3 : (b1) TEM image and (b2) a comparison of the e_g electron configuration; reproduced with permission [54] Copyright (2016), Springer Nature. (c) Exsolved nanoparticles boost the bifunctional activity of $\text{La}_{0.8}\text{Sr}_{0.2}\text{Cr}_{0.69}\text{Ni}_{0.31}\text{O}_{3-\delta}$ perovskite oxide toward the overall water splitting reaction: (c1) TEM image and (c2) cycling stability before and after 500 h of chronopotentiometry; reproduced with permission [64] Copyright (2019), Elsevier.

Distinct from conventional strategies such as infiltration, exsolution offers a unique method for growing nanoparticles in-situ from the perovskite oxide backbone [65,66]. The flexible nature of the perovskite structure can easily incorporate catalytically active elements. When exposed to a reducing environment, those elements can be partially exsolved onto the perovskite oxide surface as nanoparticles [67]. In addition, the exsolution process can be facilitated by introducing a moderate number of A-site deficiencies [68]. Perovskite oxide surfaces decorated with uniformly dispersed and catalytically active nanoparticles are favorable for excellent performance. For example, Liu and coworkers fabricated a unique surface with LSCN/ Ni_2P interfaces via exsolving Ni nanoparticles

from $\text{La}_{0.8}\text{Sr}_{0.2}\text{Cr}_{0.69}\text{Ni}_{0.31}\text{O}_{3-\delta}$ (LSCN), followed by phosphatization (see TEM (transmission electron microscope) image in Figure 3(c1)), which boosted the intrinsic OER activity ~ 6.2 -fold and the mass activity ~ 10.2 -fold. When used as a bifunctional electrocatalyst in a symmetrical two-electrode water electrolyzer, this catalyst delivered enhanced stability when compared to Pt/C-IrO₂ during a 500-h chronopotentiometry test (Figure 3(c2)) [64].

We should note that perovskite oxide supports are usually required for exsolution-prepared nanoparticles, while substrates are necessary for deposition-derived nanofilms, which potentially limits the number of active sites available. For the sake of fully utilizing the catalytic potential of the nanostructured moieties, the removal of the supporting substrate is highly desirable. Very recently, freestanding perovskite oxide thin films down to a few atomic layers were fabricated using a sacrificial buffer layer method [69], which may open up new opportunities for nanostructured perovskite oxide electrocatalysts.

2.4. Hybridization

In addition to the above-mentioned strategies used to boost the activity of perovskite oxide catalysts intrinsically by modifying their electronic structures and extrinsically by exposing more active sites, another exciting method involves hybridizing perovskite oxides with other active species. The motivation behind this approach is to expose a large number of active sites, [70] improve the electronic conductivity [71], or modify the electronic structure [72]. One example is presented in Figure 4(a1), which demonstrates the positive role of hybridization with MoS₂ in boosting the HER activity of $\text{LaNiO}_{3-\delta}$ (LNO) perovskite oxide. This enhancement in the HER activity was observed for other hybrids, including $\text{Ba}_{0.95}\text{La}_{0.05}\text{FeO}_{3-\delta}/\text{MoS}_2$ and $\text{Pr}_{0.5}(\text{Ba}_{0.5}\text{Sr}_{0.5})_{0.5}\text{Co}_{0.8}\text{Fe}_{0.2}\text{O}_{3-\delta}/\text{MoS}_2$ [73]. The increased number of heterogeneous interfaces formed upon mechanical hybridization (ball-milling) modified the surface structure of LNO, which was reflected by the positive shift observed for the Ni 3p XPS peak towards the higher binding energy region (Figure 4(a2)) [73]. The increased Ni valence state caused by hybridization contributes to the intake of hydroxyl groups due to their strong electrostatic affinity and thus, boosts the HER activity [18]. A similar improvement in the activity was observed by combining perovskite oxide with transition metal dichalcogenides in $\text{La}_{0.5}\text{Sr}_{0.5}\text{CoO}_{3-\delta}$ (LSC)/MoSe₂, which enabled stable alkaline water splitting for 1000 h without any obvious degradation in its activity (Figure 4b) [74].

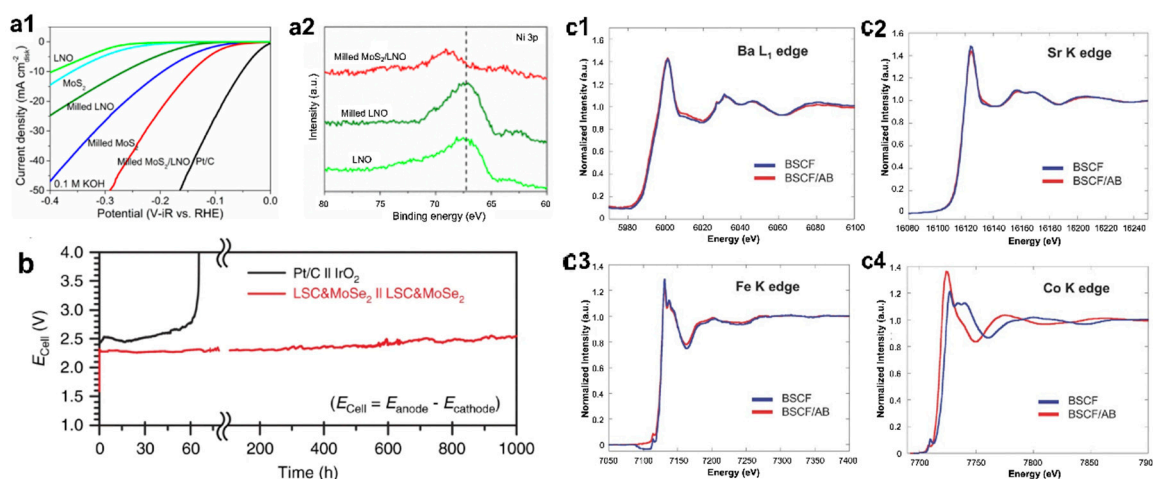


Figure 4. (a) Hybridization of perovskite oxide with MoS₂ boosts the HER activity in an alkaline electrolyte: (a1) HER polarization curves obtained in 0.1 M KOH and (a2) the Ni 3p XPS spectra obtained for LNO, milled LNO, and milled MoS₂/LNO; reproduced with permission [73] Copyright (2018), American Chemical Society. (b) Chronopotentiometric test measured at 100 mA cm⁻² for the overall water splitting reaction over 1000 h; reproduced with permission [74] Copyright (2019), Springer

Nature. (c) Conductive carbon modifies the electronic structure of BSCF. Normalized XANES (X-ray absorption near edge structure) spectra observed at the (c1) Ba L-edge, (c2) Sr K-edge, (c3) Fe K-edge, and (c4) Co K-edge; reproduced with permission [75] Copyright (2015), John Wiley and Sons.

The synthesis of crystalline perovskite oxides usually requires a high calcination temperature, where the particles tend to agglomerate and decrease the surface area [76,77]. In order to mitigate this shortcoming, perovskite oxides are usually hybridized with porous conductive carbon materials to expose more active sites [78]. In addition to functioning as a conductive support, carbon materials can influence the electronic configuration of perovskite oxides [72,75]. It was found that conductive acetylene black (AB) mixed with BSCF led to a negative shift in the Co K-edge when compared to bare BSCF (Figure 4(c4)), while maintaining comparable XANES (X-ray absorption near edge structure) fingerprints at the Ba L-edge (Figure 4(c1)), Sr K-edge (Figure 4(c2)), and Fe K-edge (Figure 4(c3)). The fact that AB carbon induces a lower mean oxidation state for the Co cations in BSCF/AB than that in BSCF indicates that it creates more oxygen vacancies, which may be the reason for its improved OER performance [75].

Defect engineering, strain tuning, nanostructuring, and hybridization are common strategies used to boost the catalytic performance of perovskite oxides. Due to these design strategies, perovskite oxides have been substantially advanced as OER and HER electrocatalysts. A summary of their activity is shown in Table 1. Rationally combining these strategies to work in a synergistic manner is suggested toward the design of superior perovskite-based water splitting electrocatalysts.

Table 1. OER (oxygen evolution reaction) and HER (hydrogen evolution reaction) activities of recently reported perovskite catalysts observed in an alkaline electrolyte.

Catalyst	Synthesis Method	OER Potential (V vs. RHE) at 10 mA cm ⁻²	HER Potential (V vs. RHE) at -10 mA cm ⁻²	Reference
NBM5.5	Reductive annealing	1.62	-0.29	[12]
PBC-1100	Sol-gel	-	-0.245	[17]
Pr0.5BSCF	Sol-gel	-	~ -0.24	[18]
C-NSCFNb	Exsolution	1.65	-0.47	[19]
LBSCF	Solid-state reaction	~1.5	~-0.02	[39]
C-NSCFNb	-	-	-	-
SNCF-NR	Electrospinning	1.62	~-0.24	[58]
LSCN-P	Exsolution & phosphatization	1.63	-0.339	[64]
MoS ₂ /LNO	Ball milling	-	~ -0.15	[73]
LSC/MoSe ₂	Ball milling	~1.6	~-0.24	[74]
Gd0.5	Sol-gel	-	~-0.21	[79]
3DOM-LF	colloidal template	1.64	~-0.4	[80]
Sr ₂ Fe ₂ O _{6-δ}	Sol-gel	1.71	/	[81]

3. Advances of Perovskite Electrocatalysts

Due to the design strategies summarized beforehand, perovskite oxides have been substantially advanced as water splitting electrocatalysts. In this chapter, we group the perovskite oxides using the 3d transition metal elements in the B-site, including Co, Ni, Fe, Mn and others, and review their most recent advances accordingly.

3.1. Co-Based

In various FDMPOs, cobalt-based perovskite oxides are the most extensively investigated for water electrolysis [82]. One of the most widely investigated Co-based perovskites is Ba_{0.5}Sr_{0.5}Co_{0.8}Fe_{0.2}O_{3-δ}, which has an optimal e_g orbital filling close to unity and intrinsic OER activity approximately one order of magnitude higher than that of IrO₂ [83]. One particularly interesting phenomenon regarding this material is that Ba_{0.5}Sr_{0.5}Co_{0.8}Fe_{0.2}O_{3-δ} experiences an in-situ surface transformation

into amorphous cobalt oxyhydroxide during the OER, leading to increased OER activity upon electrochemical cycling [84]. In addition, the amorphous perovskite surface can be facilitated by heat treatment in Ar [85], Li treatment [86], photochemical decomposition [87], etc. Recently, Fabbri and coworkers found that the in-situ surface restructuring of $\text{Ba}_{0.5}\text{Sr}_{0.5}\text{Co}_{0.8}\text{Fe}_{0.2}\text{O}_{3-\delta}$ was related to the lattice oxygen evolution reaction (LOER) process ($\text{ABO}_{3-\delta} + \text{OH}^- \leftrightarrow \text{BO}(\text{OH}) + \text{A}_{\text{aq}}^{2+} + \frac{2-\delta}{2}\text{O}_2 + 3\text{e}^-$) using operando X-ray absorption fine structure spectroscopy (XAFS) [46].

The LOER process is activated by the large oxygen vacancy content in Co-based perovskites, which improves the covalency between the Co 3d and O 2p bands (Figure 5a) and makes the oxidation of the lattice oxygen atoms thermodynamically favorable [88]. Shao-Horn and coworkers provided direct evidence for the oxidation of lattice oxygen during the OER using online electrochemical mass spectrometry (OLEMS). In their experiments, the perovskite oxides were isotopically-labeled with ^{18}O and the oxygen gas evolved by perovskite catalysts under normal KOH electrolyte conditions was monitored in-situ using OLEMS. In addition to $^{32}\text{O}_2$, $^{34}\text{O}_2$ ($^{16}\text{O}^{18}\text{O}$) and $^{36}\text{O}_2$ ($^{18}\text{O}^{18}\text{O}$) were also detected for the highly covalent $\text{SrCoO}_{3-\delta}$ catalyst, confirming the LOER process since only the isotopically-labeled perovskite oxide provided ^{18}O . A plausible mechanism explaining the formation of $^{36}\text{O}_2$ is proposed, which consists of O-O bond formation, the evolution of oxygen gas, and the generation of oxygen vacancies [88]. The verification of the LOER process updates the previous knowledge that B-site cations are only the redox centers in perovskite oxides and enriches our insight into the OER mechanisms, which can be utilized to design more OER-active perovskites.

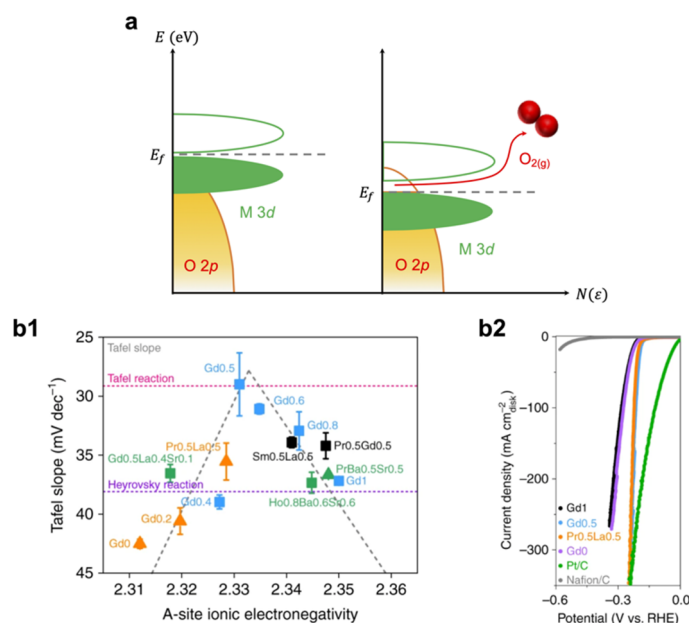


Figure 5. (a) Activating the lattice oxygen redox by improving the metal-oxygen hybridization: (a) A schematic illustration of the band structures observed for LaCoO_3 and SrCoO_3 during the OER. (b) A-site ionic electronegativity as a descriptor of perovskite oxide HER activity: (b1) The HER Tafel slope as a function of the A-site ionic electronegativity and (b2) polarization curve; reproduced with permission [79] Copyright (2019), Springer Nature.

In addition to the OER, Co-based perovskite oxides have been also used in the HER. A number of cobalt-based perovskite oxides including both simple perovskites and double perovskites have been systematically studied for the alkaline HER [79]. By changing the A-site dopants with different ionic electronegativity, the cobalt valence was facily tuned and optimized. A volcano-type relationship with thirteen different compositions was observed for the HER activity as a function of the A-site electronegativity (Figure 5(b1)), suggesting that the A-site electronegativity may serve as an HER descriptor for perovskite oxides. The highest HER activity, which was comparable to Pt/C, was achieved

at a moderate electronegativity value equal to ≈ 2.33 , in which $\text{Ba}_{0.4}\text{Ca}_{0.6}\text{Gd}_{0.4}\text{La}_{0.6}\text{Co}_2\text{O}_{5.5+\delta}$ and $\text{Ba}_{0.5}\text{Ca}_{0.5}\text{Pr}_{0.5}\text{La}_{0.5}\text{Co}_2\text{O}_{5.5+\delta}$ achieved optimal Co valence and band structures (Figure 5(b2)) [79].

3.2. Ni-Based

Even though Co-based perovskite oxides have shown promising OER and HER activities, the relatively high price of cobalt is unfavorable for their large-scale application. When compared with Co, many other first d-block transition metals, such as Ni, Mn, and Fe, are significantly cheaper (Scheme 1). As a result, they are also frequently investigated for water electrolysis [89]. One popular Ni-based perovskite oxide is LaNiO_3 [90], which is a well-known conducting perovskite oxide. Its high electronic conductivity ($1000 \Omega^{-1} \text{ cm}^{-1}$ at room temperature) is expected to favor the charge transfer kinetics required during electrolysis, eliminating the need for a conductive carbon support, which affects the catalytic activity [91]. Bulk LaNiO_3 is superior to Pt in catalyzing the OER [92], even though its OER activity is still inferior to that observed for more active NiCoO_x and RuO_2 [93,94]. In order to further enhance the catalytic activity of LaNiO_3 , strategies such as Fe-doping [89,95], strain tuning [96], and oxygen vacancy engineering [97] have been investigated to date. It is worth noting that these strategies can perturb or distort the octahedral geometry of BO_6 . Identifying this perturbation and further clarifying its role in water electrolysis are imperative. Chung and coworkers visualized the atomic-scale perturbation of the octahedral oxygen atoms in LaNiO_3 thin films using high-resolution scanning transmission electron microscopy (STEM), as shown in Figure 6(a1). In contrast to the bulk where four oxygen atoms were placed at the corners of a white rhombus for a Ni octahedron, the surface unit cells denoted by the yellow rhombus were substantially distorted. The strong distortions in the oxygen octahedron were generated by the surface exchange of Ni with Fe, which enhanced the OER activity by several orders of magnitude. Density functional theory (DFT) calculations further demonstrated that this atomic-scale structural perturbation changes the O 2p and Ni/Fe 3d states in particular near the Fermi level (from -2 to 0 eV), as shown in Figure 6(a2,a3), leading to facile charge transfer between the metal and oxygen atoms [98].

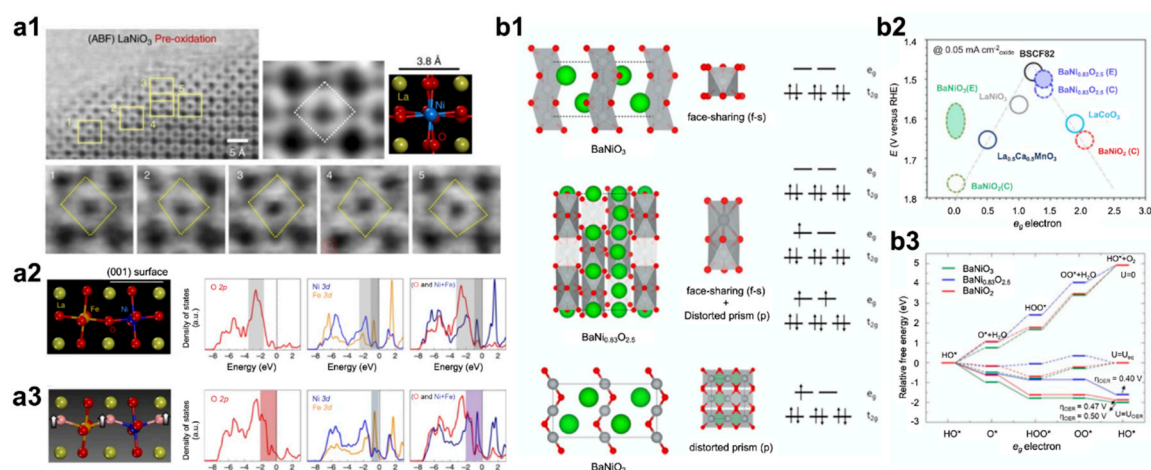


Figure 6. (a) Perturbation of oxygen octahedral in LaNiO_3 activates the water oxidation reaction: (a1) STEM image of the distorted oxygen octahedron; and a (density of states) DOS comparison between Fe-doped (001) LaNiO_3 (a2) without and (a3) with distorted octahedral oxygen atoms; reproduced with permission [98] Copyright (2019), Springer Nature. (b) $\text{BaNi}_{0.83}\text{O}_{2.5}$ as a superior OER electrocatalyst: (b1) structures of BaNiO_3 , $\text{BaNi}_{0.83}\text{O}_{2.5}$, and BaNiO_2 , (b2) OER activity as a function of the e_g orbital occupancy, and (b3) DFT-calculated free energy diagrams; reproduced with permission [99] Copyright (2016), American Chemical Society.

Notably, Ni-based perovskite oxides can also undergo a structural transformation during electrolysis. One representative example is BaNiO_3 [99], which has a hexagonal structure with

face-shared octahedral NiO_6 oriented toward the chain units, as shown in Figure 6(b1). During the OER cycling process, BaNiO_3 was transformed into $\text{BaNi}_{0.83}\text{O}_{2.5}$ ($\text{Ba}_6\text{Ni}_5\text{O}_{15}$), which has mixed valence states of Ni^{2+} , Ni^{3+} , and Ni^{4+} with distorted-prism coordinations (Figure 6(b1)). Due to these structural transformations, the OER activity of BaNiO_3 was improved substantially, even far beyond the state-of-the-art IrO_2 catalyst (Figure 6(b2)). From the DFT calculations shown in Figure 6(b3), $\text{BaNi}_{0.83}\text{O}_{2.5}$ requires a smaller overpotential to make all the OER sub-steps downhill when compared to BaNiO_3 , supporting its higher OER activity [99]. Several Ni-based perovskite oxides have been introduced with promising OER activities. However, their use as HER electrocatalysts has seldom been investigated and awaits future effort.

3.3. Fe-Based

Considering the abundance of Fe in the earth's crust is far larger than that of Co and Ni, it is appealing to develop Fe-based perovskite electrocatalysts with comparable activity to their Co- and Ni-based counterparts. Fe is usually incorporated into Co- or Ni-based catalysts to boost the catalytic performance [5,94]. However, Fe-based perovskites, in which Fe acts as a single active site, have not been investigated as broadly as their Co- and Ni-based counterparts. This is mainly due to the low intrinsic activity of Fe-based perovskite oxides [100]. Recent efforts have been devoted to improving the catalytic performance of Fe-based perovskite oxides [70,101]. A series of Fe-based perovskite oxides including $\text{Ca}_2\text{Fe}_2\text{O}_{6-\delta}$, $\text{CaSrFe}_2\text{O}_{6-\delta}$, and $\text{Sr}_2\text{Fe}_2\text{O}_{6-\delta}$, which have different structures (Figure 7(a1)) have been compared in the OER. The tetrahedral chains in each layer of $\text{Ca}_2\text{Fe}_2\text{O}_{6-\delta}$ are oriented in an opposite direction to their neighboring layers, which is in contrast to $\text{CaSrFe}_2\text{O}_{6-\delta}$ where the tetrahedral chains are orientated in the same direction. $\text{Sr}_2\text{Fe}_2\text{O}_{6-\delta}$ has a different type of defect order with alternating square pyramidal and octahedral coordination. These unique structures render distinct electronic conductivities. The room temperature conductivities determined using 4-probe measurements followed the order of: $\text{Ca}_2\text{Fe}_2\text{O}_{6-\delta}$ ($1.13 \times 10^{-9} \text{ S cm}^{-1}$) < $\text{CaSrFe}_2\text{O}_{6-\delta}$ ($7.78 \times 10^{-3} \text{ S cm}^{-1}$) < $\text{Sr}_2\text{Fe}_2\text{O}_{6-\delta}$ (7.30 S cm^{-1}). With the highest conductivity favorable for the charge transfer process, $\text{Sr}_2\text{Fe}_2\text{O}_{6-\delta}$ exhibited the best OER activity [81].

In addition to optimizing the conductivity, another strategy is to increase the proportion of Fe^{4+} to improve the binding strength with the reaction intermediates [102,103]. Even though cationic and anionic dopants have been introduced into the perovskite framework to provoke Fe^{4+} [34], stabilizing most or even all of the Fe cations in the tetravalent state remains challenging. A quadruple $\text{AA}'_3\text{B}_4\text{O}_{12}$ -type perovskite structure ($\text{CaCu}_3\text{Fe}_4\text{O}_{12}$) has been applied to accommodate Fe^{4+} [11]. In this type of perovskite structure, the A-sites are occupied by alkaline/alkaline-earth/rare-earth metal ions, the A'-sites are occupied by Jahn-Teller active ions such as Cu^{2+} or Mn^{3+} , and the B-sites contain d-block transition metal ions (Figure 7(b1)). The intrinsic OER activity (normalized by surface area) of $\text{CaCu}_3\text{Fe}_4\text{O}_{12}$ exceeds that of the state-of-the-art BSCF and RuO_2 (Figure 7(b2)), demonstrating its great potential for water electrolysis. The tetravalent Fe atoms in $\text{CaCu}_3\text{Fe}_4\text{O}_{12}$ improved the covalency of the transition metal-oxygen bonds and shortened the interatomic distance between the nearest neighboring OH adsorbates (Figure 7(a3)), making the formation of O–O bonds possible, which is regarded as the rate-limiting step in the OER [11].

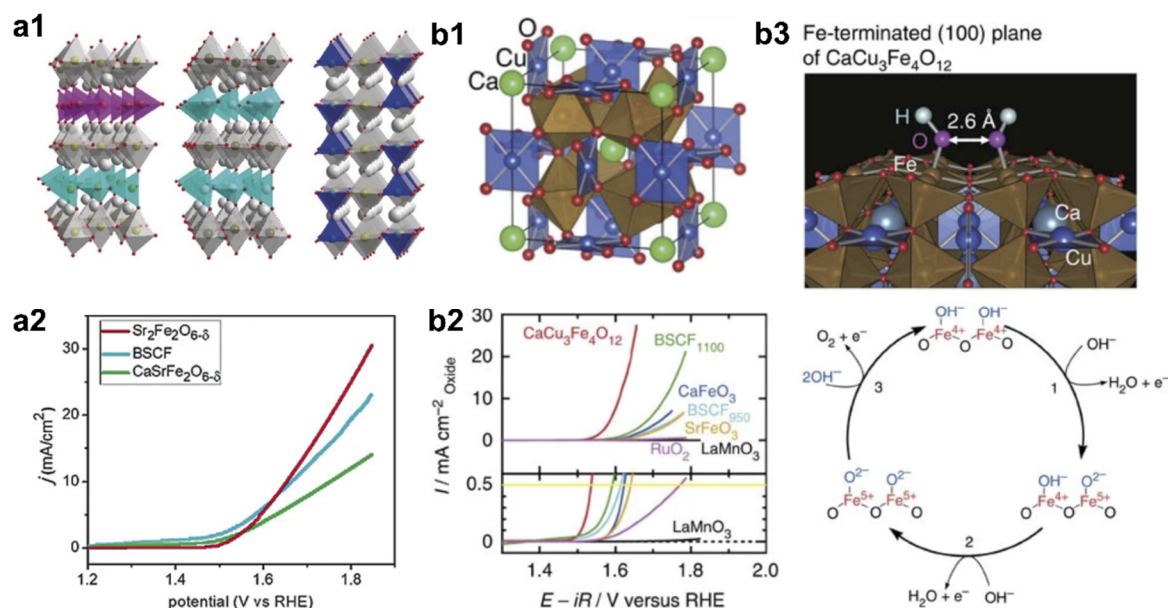


Figure 7. (a) Highly electronically-conductive Fe-based OER electrocatalysts: (a1) The crystal structures (from left to right) of $\text{Ca}_2\text{Fe}_2\text{O}_{6-\delta}$, $\text{CaSrFe}_2\text{O}_{6-\delta}$, and $\text{Sr}_2\text{Fe}_2\text{O}_{6-\delta}$, and (a2) the OER activity tested without a conductive carbon additive; reproduced with permission [81] Copyright (2019), John Wiley and Sons. (b) Covalency-reinforced Fe^{4+} -based quadruple perovskite $\text{CaCu}_3\text{Fe}_4\text{O}_{12}$ OER electrocatalysts: (b1) A structural illustration of $\text{CaCu}_3\text{Fe}_4\text{O}_{12}$, (b2) geometric OER activity, and (b3) potential OER pathway on the surface of $\text{CaCu}_3\text{Fe}_4\text{O}_{12}$; reproduced with permission [11] Copyright (2015), Springer Nature.

3.4. Mn-Based

Mn-based oxides, especially CaMn oxides, have recently gained a significant amount of interest as water oxidation catalysts due to their similarity to the natural oxygen-evolving cluster (CaMn_4O_5) found in photosynthetic plant cells [104,105]. In addition, the high abundance and low cost of Mn have also helped attract interest for use as electrocatalysts. However, the catalytic activity of Mn-based perovskite oxides is typically low and almost inert [71,106]. One of the widely known methods to boost the catalytic performance of Mn-based perovskite oxides is to increase the oxygen vacancy concentration [107,108]. The motivation behind this strategy is to facilitate the intake of hydroxyl groups, which should readily adsorb on the oxygen vacant sites in the Mn-perovskite oxide (Figure 8(a1)) [43]. One representative example is orthorhombic $\text{Ca}_2\text{Mn}_2\text{O}_5$, which has five-coordinated square pyramid subunits composed of manganese and oxygen (Figure 8(a2)). In contrast, orthorhombic CaMnO_3 without oxygen vacancies has six-coordinated octahedral subunits. The OER activity of $\text{Ca}_2\text{Mn}_2\text{O}_5$ was significantly improved due to these oxygen vacancies [43].

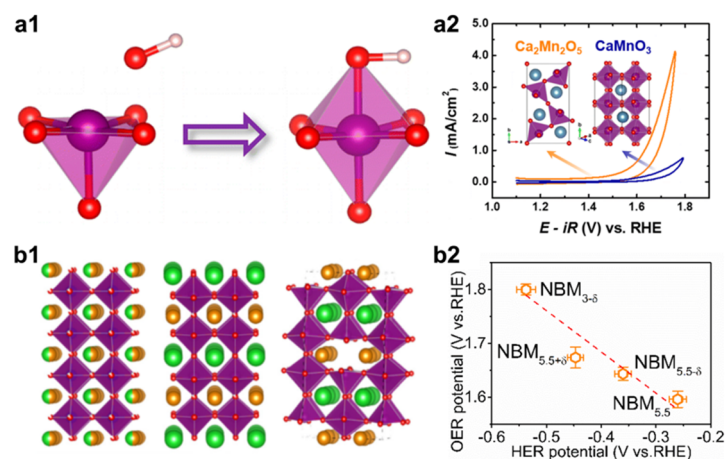


Figure 8. (a) Oxygen-deficient $\text{Ca}_2\text{Mn}_2\text{O}_5$ perovskite as an OER electrocatalyst: (a1) The plausible effect of the oxygen vacancies in $\text{Ca}_2\text{Mn}_2\text{O}_5$ on the OER kinetics and (a2) the structure and OER CV; reproduced with permission [43] Copyright (2014), American Chemical Society. (b) Orthorhombic $\text{NdBaMn}_2\text{O}_{5.5}$ as a bifunctional OER and HER catalyst: (b1) The structure (from the left to the right) of $\text{Nd}_{0.5}\text{Ba}_{0.5}\text{MnO}_{3-\delta}$, $\text{NdBaMn}_2\text{O}_{5.5-\delta}$, and $\text{NdBaMn}_2\text{O}_{5.5}$ and (b2) the OER and HER onset potential obtained at 0.5 mA cm^{-2} ; reproduced with permission [12] Copyright (2018), American Chemical Society.

In addition to improving the adsorption of the hydroxyl groups, the oxygen vacancies can also cause structural transformations within Mn-based perovskite oxides and affects water electrolysis performance. In a recent study, Wang and coworkers demonstrated that perovskite oxides with ordered oxygen vacancies can achieve enhanced HER and OER activity in an alkaline electrolyte [12]. In their study, $\text{Nd}_{0.5}\text{Ba}_{0.5}\text{MnO}_{3-\delta}$ ($\text{NBM}_{3-\delta}$) was used as the parent material and a series of perovskites with different structures and oxygen vacancy concentrations were easily obtained by extending the reductive annealing time, including $\text{NdBaMn}_2\text{O}_{5.5+\delta}$ ($\text{NBM}_{5.5+\delta}$, where $\delta < 0.5$), $\text{NdBaMn}_2\text{O}_{5.5}$ ($\text{NBM}_{5.5}$), and $\text{NdBaMn}_2\text{O}_{5.5-\delta}$ ($\text{NBM}_{5.5-\delta}$, where $\delta < 0.5$) [12]. Upon reduction, the partial removal of crystalline oxygen and an increased number of oxygen vacancies ($2\text{Mn}_{\text{Mn}} + \text{O}_{\text{Ox}} \rightarrow 1/2\text{O}_2 + \text{V}_{\text{O}} + 2\text{Mn}_{\text{MnX}}$) forces the A-site cations to be ordered; the layers of Nd-O and Ba-O are alternated along the c-axis, in which the oxygen vacancies were disorderly localized in the Nd-O layer. However, when the oxygen non-stoichiometry reached 0.5, MO_5 square pyramids and MO_6 octahedra were alternated periodically along the b-axis, generating orderly distributed oxygen vacancies. The detailed structures are displayed in Figure 8(b1). This unique arrangement of orderly distributed oxygen vacancies endowed $\text{NBM}_{5.5}$ with a half-filled e_g orbital, optimized O p-band, and distorted structure, which significantly improves the OER and HER activity, as shown in Figure 8(b2). However, it should be noted that Mn-based perovskite oxides exhibit far from satisfactory catalytic performance. The OER and HER activity are still inferior to those observed for their commercial counterparts and future efforts are required to further enhance their activity.

3.5. Other First d-Block Metal-Based

More than Co, Ni, Fe, Mn, other first d-block metal-based (e.g., V, Cr, Cu, Ti) perovskite oxides have also been studied for water electrolysis [109–112]. Recently, a systematic study of simple perovskite oxides used as OER catalysts has been conducted by Yagi and coworkers [113]. 25 kinds of perovskite oxide catalysts including CaBO_3 ($\text{B} = \text{Ti, V, Cr, Mn, Fe, and Co}$), SrBO_3 ($\text{B} = \text{Ti, V, Cr, Mn, Fe, and Co}$), YBO_3 ($\text{B} = \text{V, Cr, Mn, Fe, Co, and Ni}$), and LaBO_3 ($\text{B} = \text{V, Cr, Mn, Fe, Co, Ni, and Cu}$) were experimentally compared in the OER and their overpotentials displayed in Figure 9(a1) (except for some extremely inert compositions). From the comparison, V-, Cr-, Cu-, and Ti-based perovskite oxides are not that competitive when compared to their Co/Ni/Fe counterparts with similar structures. In addition to the activity comparison, several OER activity descriptors were examined for the 25 perovskite oxides,

including e_g orbital filling, oxygen 2p band center relative to the Fermi energy, and charge-transfer energy. In contrast to the e_g orbital occupancy and oxygen 2p band location, only the charge-transfer energy was found to display a linear relationship with the OER overpotential and can serve as the most helpful descriptor for the OER [113].

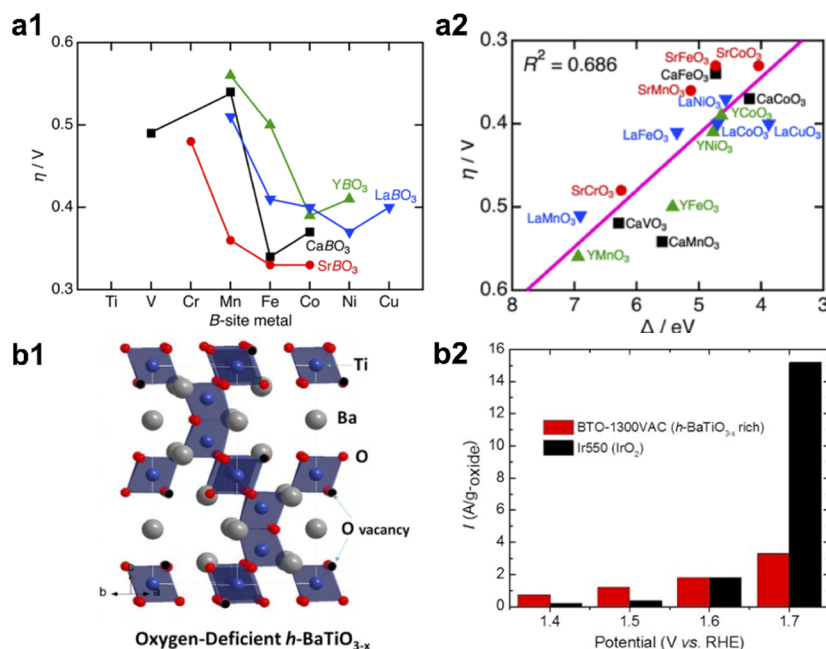


Figure 9. (a) Systematic comparison of various first d-block metal-based perovskite oxides used for the OER: (a1) A comparison of the OER overpotential and (a2) the OER overpotential as a function of the charge transfer energy; reproduced with permission [113] Copyright (2014), American Chemical Society. Oxygen-deficient BaTiO_{3- δ} as a highly-active OER electrocatalyst: (b1) A structural illustration of BaTiO_{3- δ} and (b2) a comparison of the OER mass activity between BaTiO_{3- δ} and Ir550; reproduced with permission [114] Copyright (2015), Elsevier.

From the above study, there is great scope to boost the catalytic activity of V-, Cr-, Cu-, and Ti-based perovskite oxides. Recent studies have shown that BaTiO_{3- δ} is a promising candidate for the OER [114,115]. BaTiO_{3- δ} nanoparticles with a large oxygen vacancy concentration have been fabricated using a sol-gel method. A number of oxygen vacancies stabilize the hexagonal structure of BaTiO_{3- δ} , where the TiO₆ octahedra share both corners and faces (Figure 9(b1)). BaTiO_{3- δ} outperformed the IrO₂ catalyst in the OER at relatively low potentials (<1.6 V) with a reduced onset potential (1.32 V vs. RHE) and an increased current density (Figure 9(b2)). The OER activity of BaTiO_{3- δ} can be further improved upon Fe- and Ni-doping by boosting the electronic conductivity [116].

4. Perspectives and Challenges

In this review, we have provided an in-time summary of the current advances in first d-block perovskite oxide-based water splitting electrocatalysts, in which the popular design strategies used to boost their activity have also been elaborated. Great strides have been made with many promising perovskite-type electrocatalysts exhibiting activities comparable or superior to those of commercial electrocatalysts have been designed and new theories involving the lattice-oxygen-evolution-mediated process have been experimentally confirmed. These will be beneficial to better understanding and further developing first d-block perovskite oxide electrocatalysts. However, many challenges still remain to be addressed:

1. More precise control over the perovskite composition, structure, and active sites is required. Despite the fact that strategies such as defect engineering, strain tuning, and hybridization

have proven effective to modulate the electronic structure and boost the intrinsic activity, precisely modulating the specific doping/strain/interface sites and configuration still have major difficulties. In addition, we should note that many perovskite-type electrocatalysts undergo in-situ surface reconstruction during water electrolysis [37,99], which makes the identification of their active sites quite complicated. As a result, advanced in-situ/operando experimental tools are required to monitor the dynamic changes observed in perovskite oxide electrocatalysts during water electrolysis, elucidate their catalytic mechanism, and identify their active sites. DFT calculations provide effective theoretical tools to understand and predict the active species/configurations in perovskite oxide electrocatalysts. However, DFT calculations are subject to many approximations. In addition, it is also quite challenging for current theoretical modeling to precisely describe the working conditions of an electrocatalyst and rationally correlate the composition, structure, and morphology with the apparent activity. Further efforts are required to continuously optimize DFT methods to better model the real working conditions, improve the calculation accuracy, and reduce the computational cost.

2. The catalytic performance of perovskite-type water splitting electrocatalysts is far from satisfactory. Although many perovskite compositions have been reported to outperform Ru- or Ir-based electrocatalysts in catalyzing the OER, the alkaline HER activity of many perovskite oxides is still far below that of Pt metal/alloys. In addition, promising OER activity has been reported for Co-based perovskite oxides, which are relatively expensive. Developing other first d-block metal perovskite oxides (e.g., Fe, Mn, Cu) with comparable activity to Co-based perovskite oxide are favorable to save the cost, which, in turn, accelerates their practical applications. In addition to the half-cell OER/HER test, it is very crucial to build the practical water electrolyzer and exam the realistic performance where other practical and yet-unsolved issues such as the durability and catalyst loading can be clearly identified. Thus, catalytic stability is another imperative factor that should be further improved besides the activity.

In conclusion, there is still a long way to go before the large-scale utilization of perovskite oxides as bifunctional electrocatalysts in alkaline water splitting. With cooperative efforts from the research community, the revolution of perovskite-type water splitting electrocatalysts will be foreseen.

Author Contributions: J.W. proposes the review topic and writes the whole text; S.C. searches and collects all the literatures; J.K. makes the plots; S.W.C. and J.L. revise the manuscript. All authors have read and agreed to the published version of the manuscript.

Funding: This research and the APC were funded by Research Resettlement Fund for the new faculty of Seoul National University (SNU) (No. 305-20170013), by the National Research Foundation of Korea (NRF) grant funded by the Korea government (MSIT) (No. NRF-2018M1A2A2063868, NRF-2019R1A4A1025848, and NRF-2019M3E6A1065102), and also by the Creative Materials Discovery Program through the National Research Foundation of Korea (NRF), funded by Ministry of Science and ICT (No. 2015M3D1A1070639).

Acknowledgments: The authors gratefully acknowledge the support of the Research Resettlement Fund for the new faculty of Seoul National University (SNU) (No. 305-20170013). This research was supported by the National Research Foundation of Korea (NRF) grant funded by the Korea government (MSIT) (No. NRF-2018M1A2A2063868, NRF-2019R1A4A1025848, and NRF-2019M3E6A1065102), and also by the Creative Materials Discovery Program through the National Research Foundation of Korea (NRF), funded by Ministry of Science and ICT (No. 2015M3D1A1070639).

Conflicts of Interest: The authors declare no conflict of interest.

References

1. Bockris, J.O.M. Kinetics of activation controlled consecutive electrochemical reactions: Anodic evolution of oxygen. *J. Chem. Phys.* **1956**, *24*, 817–827. [[CrossRef](#)]
2. Shinagawa, T.; Garcia-Esparza, A.T.; Takanabe, K. Insight on Tafel slopes from a microkinetic analysis of aqueous electrocatalysis for energy conversion. *Sci. Rep.* **2015**, *5*, 13801. [[CrossRef](#)] [[PubMed](#)]
3. Faid, A.Y.; Oyarce Barnett, A.; Seland, F.; Sunde, S. Highly active nickel-based catalyst for hydrogen evolution in anion exchange membrane electrolysis. *Catalysts* **2018**, *8*, 614. [[CrossRef](#)]

4. Brauns, J.; Turek, T. Alkaline water electrolysis powered by renewable energy: A review. *Processes* **2020**, *8*, 248. [CrossRef]
5. Wang, J.; Ciucci, F. In-situ synthesis of bimetallic phosphide with carbon tubes as an active electrocatalyst for oxygen evolution reaction. *Appl. Catal. B Environ.* **2019**, *254*, 292–299. [CrossRef]
6. Wang, T.; Chen, H.; Yang, Z.; Liang, J.; Dai, S. High-Entropy Perovskite Fluorides: A New Platform for Oxygen Evolution Catalysis. *J. Am. Chem. Soc.* **2020**, *142*, 4550–4554. [CrossRef]
7. Li, B.-Q.; Tang, C.; Wang, H.-F.; Zhu, X.-L.; Zhang, Q. An aqueous preoxidation method for monolithic perovskite electrocatalysts with enhanced water oxidation performance. *Sci. Adv.* **2016**, *2*, e1600495. [CrossRef]
8. Montoya, J.H.; Doyle, A.D.; Nørskov, J.K.; Vojvodic, A. Trends in adsorption of electrocatalytic water splitting intermediates on cubic ABO₃ oxides. *Phys. Chem. Chem. Phys.* **2018**, *20*, 3813–3818. [CrossRef]
9. Xu, J.; Chen, C.; Han, Z.; Yang, Y.; Li, J.; Deng, Q. Recent Advances in Oxygen Electrocatalysts Based on Perovskite Oxides. *Nanomaterials* **2019**, *9*, 1161. [CrossRef]
10. Liu, S.; Luo, H.; Li, Y.; Liu, Q.; Luo, J.-L. Structure-engineered electrocatalyst enables highly active and stable oxygen evolution reaction over layered perovskite LaSr₃Co_{1.5}Fe_{1.5}O_{10-δ}. *Nano Energy* **2017**, *40*, 115–121. [CrossRef]
11. Yagi, S.; Yamada, I.; Tsukasaki, H.; Seno, A.; Murakami, M.; Fujii, H.; Chen, H.; Umezawa, N.; Abe, H.; Nishiyama, N. Covalency-reinforced oxygen evolution reaction catalyst. *Nat. Commun.* **2015**, *6*, 8249. [CrossRef] [PubMed]
12. Wang, J.; Gao, Y.; Chen, D.; Liu, J.; Zhang, Z.; Shao, Z.; Ciucci, F. Water Splitting with an Enhanced Bifunctional Double Perovskite. *ACS Catal.* **2018**, *8*, 364–371. [CrossRef]
13. Lee, D.; Lee, H.N. Controlling oxygen mobility in Ruddlesden–Popper oxides. *Materials* **2017**, *10*, 368. [CrossRef] [PubMed]
14. Calle-Vallejo, F.; Inoglu, N.G.; Su, H.-Y.; Martínez, J.I.; Man, I.C.; Koper, M.T.; Kitchin, J.R.; Rossmeisl, J. Number of outer electrons as descriptor for adsorption processes on transition metals and their oxides. *Chem. Sci.* **2013**, *4*, 1245–1249. [CrossRef]
15. Lam, K.; Gao, Y.; Wang, J.; Ciucci, F. H₂O₂ Treated La_{0.8}Sr_{0.2}CoO_{3-δ} as an Efficient Catalyst for Oxygen Evolution Reaction. *Electrochim. Acta* **2017**, *244*, 139–145. [CrossRef]
16. Du, X.; Ai, H.; Chen, M.; Liu, D.; Chen, S.; Wang, X.; Lo, K.H.; Pan, H. PLD-fabricated perovskite oxide nanofilm as efficient electrocatalyst with highly enhanced water oxidation performance. *Appl. Catal. B Environ.* **2020**, *272*, 119046. [CrossRef]
17. Sun, Q.; Dai, Z.; Zhang, Z.; Chen, Z.; Lin, H.; Gao, Y.; Chen, D. Double perovskite PrBaCo₂O_{5.5}: An efficient and stable electrocatalyst for hydrogen evolution reaction. *J. Power Sources* **2019**, *427*, 194–200. [CrossRef]
18. Xu, X.; Chen, Y.; Zhou, W.; Zhu, Z.; Su, C.; Liu, M.; Shao, Z. A perovskite electrocatalyst for efficient hydrogen evolution reaction. *Adv. Mater.* **2016**, *28*, 6442–6448. [CrossRef]
19. Bu, Y.; Kim, S.; Kwon, O.; Zhong, Q.; Kim, G. A Composite Catalyst Based on Perovskites for Overall Water Splitting in Alkaline Conditions. *ChemElectroChem* **2019**, *6*, 1520–1524. [CrossRef]
20. Wang, H.; Zhou, M.; Choudhury, P.; Luo, H. Perovskite oxides as bifunctional oxygen electrocatalysts for oxygen evolution/reduction reactions—A mini review. *Appl. Mater. Today* **2019**, *16*, 56–71. [CrossRef]
21. Hwang, J.; Rao, R.R.; Giordano, L.; Katayama, Y.; Yu, Y.; Shao-Horn, Y. Perovskites in catalysis and electrocatalysis. *Science* **2017**, *358*, 751–756. [CrossRef] [PubMed]
22. Prices of Chemical Elements. Available online: https://en.wikipedia.org/wiki/Prices_of_chemical_elements (accessed on 25 June 2020).
23. Wang, J. Engineering Defective Electrode Materials for Sustainable Energy Applications. Ph.D. Thesis, Hong Kong University of Science and Technology, Hong Kong, China, 2018.
24. Zhang, Z.; Chen, Y.; Dai, Z.; Tan, S.; Chen, D. Promoting hydrogen-evolution activity and stability of perovskite oxides via effectively lattice doping of molybdenum. *Electrochim. Acta* **2019**, *312*, 128–136. [CrossRef]
25. Wang, J.; Saccoccio, M.; Chen, D.; Gao, Y.; Chen, C.; Ciucci, F. The effect of A-site and B-site substitution on BaFeO_{3-δ}: An investigation as a cathode material for intermediate-temperature solid oxide fuel cells. *J. Power Sources* **2015**, *297*, 511–518. [CrossRef]

26. Wang, J.; Lam, K.Y.; Saccoccio, M.; Gao, Y.; Chen, D.; Ciucci, F. Ca and In co-doped BaFeO_{3-δ} as a cobalt-free cathode material for intermediate-temperature solid oxide fuel cells. *J. Power Sources* **2016**, *324*, 224–232. [\[CrossRef\]](#)
27. Li, B.-Q.; Xia, Z.-J.; Zhang, B.; Tang, C.; Wang, H.-F.; Zhang, Q. Regulating p-block metals in perovskite nanodots for efficient electrocatalytic water oxidation. *Nat. Commun.* **2017**, *8*, 934. [\[CrossRef\]](#) [\[PubMed\]](#)
28. Alkan, B.; Medina, D.; Landers, J.; Heidelmann, M.; Hagemann, U.; Salamon, S.; Andronesco, C.; Wende, H.; Schulz, C.; Schuhmann, W.; et al. Spray-Flame-Prepared LaCo_{1-x}Fe_xO₃ Perovskite Nanoparticles as Active OER Catalysts: Influence of Fe Content and Low-Temperature Heating. *ChemElectroChem* **2020**, *7*, 2564–2574. [\[CrossRef\]](#)
29. Wang, Z.; You, Y.; Yuan, J.; Yin, Y.-X.; Li, Y.-T.; Xin, S.; Zhang, D. Nickel-Doped La_{0.8}Sr_{0.2}Mn_{1-x}Ni_xO₃ Nanoparticles Containing Abundant Oxygen Vacancies as an Optimized Bifunctional Catalyst for Oxygen Cathode in Rechargeable Lithium—Air Batteries. *ACS Appl. Mater. Interfaces* **2016**, *8*, 6520–6528. [\[CrossRef\]](#)
30. Guo, Y.; Tong, Y.; Chen, P.; Xu, K.; Zhao, J.; Lin, Y.; Chu, W.; Peng, Z.; Wu, C.; Xie, Y. Engineering the Electronic State of a Perovskite Electrocatalyst for Synergistically Enhanced Oxygen Evolution Reaction. *Adv. Mater.* **2015**, *27*, 5989–5994. [\[CrossRef\]](#)
31. Zhao, Y.; Hang, Y.; Zhang, Y.; Wang, Z.; Yao, Y.; He, X.; Zhang, C.; Zhang, D. Strontium-doped perovskite oxide La_{1-x}Sr_xMnO₃ (x = 0, 0.2, 0.6) as a highly efficient electrocatalyst for nonaqueous Li-O₂ batteries. *Electrochim. Acta* **2017**, *232*, 296–302. [\[CrossRef\]](#)
32. Zhang, Z.; Chen, D.; Wang, J.; Tan, S.; Yu, X.; Shao, Z. Highly Active and Stable Cobalt-Free Hafnium-doped SrFe_{0.9}Hf_{0.1}O_{3-δ} Perovskite Cathode for Solid Oxide Fuel Cells. *ACS Appl. Energy Mater.* **2018**, *1*, 2134–2142. [\[CrossRef\]](#)
33. Liu, J.; Wang, J.; Belotti, A.; Ciucci, F. P-Substituted Ba_{0.95}La_{0.05}FeO_{3-δ} as a Cathode Material for SOFCs. *ACS Appl. Energy Mater.* **2019**, *2*, 5472–5480. [\[CrossRef\]](#)
34. Li, Z.; Lv, L.; Wang, J.; Ao, X.; Ruan, Y.; Zha, D.; Hong, G.; Wu, Q.; Lan, Y.; Wang, C.; et al. Engineering phosphorus-doped LaFeO_{3-δ} perovskite oxide as robust bifunctional oxygen electrocatalysts in alkaline solutions. *Nano Energy* **2018**, *47*, 199–209. [\[CrossRef\]](#)
35. Xiong, J.; Zhong, H.; Li, J.; Zhang, X.; Shi, J.; Cai, W.; Qu, K.; Zhu, C.; Yang, Z.; Beckman, S.P.; et al. Engineering highly active oxygen sites in perovskite oxides for stable and efficient oxygen evolution. *Appl. Catal. B Environ.* **2019**, *256*, 117817. [\[CrossRef\]](#)
36. Duan, Y.; Sun, S.; Xi, S.; Ren, X.; Zhou, Y.; Zhang, G.; Yang, H.; Du, Y.; Xu, Z.J. Tailoring the Co 3d-O 2p Covalency in LaCoO₃ by Fe Substitution To Promote Oxygen Evolution Reaction. *Chem. Mater.* **2017**, *29*, 10534–10541. [\[CrossRef\]](#)
37. Kim, B.-J.; Fabbri, E.; Abbott, D.F.; Cheng, X.; Clark, A.H.; Nachttegaal, M.; Borlaf, M.; Castelli, I.E.; Graule, T.; Schmidt, T.J. Functional Role of Fe-Doping in Co-Based Perovskite Oxide Catalysts for Oxygen Evolution Reaction. *J. Am. Chem. Soc.* **2019**, *141*, 5231–5240. [\[CrossRef\]](#)
38. Seo, M.H.; Park, H.W.; Lee, D.U.; Park, M.G.; Chen, Z. Design of Highly Active Perovskite Oxides for Oxygen Evolution Reaction by Combining Experimental and ab Initio Studies. *ACS Catal.* **2015**, *5*, 4337–4344. [\[CrossRef\]](#)
39. Hua, B.; Li, M.; Pang, W.; Tang, W.; Zhao, S.; Jin, Z.; Zeng, Y.; Shalchi Amirkhiz, B.; Luo, J.-L. Activating p-Blocking Centers in Perovskite for Efficient Water Splitting. *Chem* **2018**, *4*, 2902–2916. [\[CrossRef\]](#)
40. Zhu, Y.; Zhou, W.; Yu, J.; Chen, Y.; Liu, M.; Shao, Z. Enhancing electrocatalytic activity of perovskite oxides by tuning cation deficiency for oxygen reduction and evolution reactions. *Chem. Mater.* **2016**, *28*, 1691–1697. [\[CrossRef\]](#)
41. Yan, L.; Lin, Y.; Yu, X.; Xu, W.; Salas, T.; Smallidge, H.; Zhou, M.; Luo, H. La_{0.8}Sr_{0.2}MnO₃-Based Perovskite Nanoparticles with the A-Site Deficiency as High Performance Bifunctional Oxygen Catalyst in Alkaline Solution. *ACS Appl. Mater. Interfaces* **2017**, *9*, 23820–23827. [\[CrossRef\]](#)
42. Bian, J.; Li, Z.; Li, N.; Sun, C. Oxygen Deficient LaMn_{0.75}Co_{0.25}O_{3-δ} Nanofibers as an Efficient Electrocatalyst for Oxygen Evolution Reaction and Zinc—Air Batteries. *Inorg. Chem.* **2019**, *58*, 8208–8214. [\[CrossRef\]](#)
43. Kim, J.; Yin, X.; Tsao, K.-C.; Fang, S.; Yang, H. Ca₂Mn₂O₅ as Oxygen-Deficient Perovskite Electrocatalyst for Oxygen Evolution Reaction. *J. Am. Chem. Soc.* **2014**, *136*, 14646–14649. [\[CrossRef\]](#)
44. Hu, C.; Wang, X.; Yao, T.; Gao, T.; Han, J.; Zhang, X.; Zhang, Y.; Xu, P.; Song, B. Enhanced Electrocatalytic Oxygen Evolution Activity by Tuning Both the Oxygen Vacancy and Orbital Occupancy of B-Site Metal Cation in NdNiO₃. *Adv. Funct. Mater.* **2019**, *29*, 1902449. [\[CrossRef\]](#)

45. Miao, X.; Wu, L.; Lin, Y.; Yuan, X.; Zhao, J.; Yan, W.; Zhou, S.; Shi, L. The role of oxygen vacancies in water oxidation for perovskite cobalt oxide electrocatalysts: Are more better? *Chem. Commun.* **2019**, *55*, 1442–1445. [[CrossRef](#)] [[PubMed](#)]
46. Fabbri, E.; Nachtegaal, M.; Binninger, T.; Cheng, X.; Kim, B.-J.; Durst, J.; Bozza, F.; Graule, T.; Schäublin, R.; Wiles, L.; et al. Dynamic surface self-reconstruction is the key of highly active perovskite nano-electrocatalysts for water splitting. *Nat. Mater.* **2017**, *16*, 925–931. [[CrossRef](#)] [[PubMed](#)]
47. Petrie, J.R.; Jeen, H.; Barron, S.C.; Meyer, T.L.; Lee, H.N. Enhancing Perovskite Electrocatalysis through Strain Tuning of the Oxygen Deficiency. *J. Am. Chem. Soc.* **2016**, *138*, 7252–7255. [[CrossRef](#)] [[PubMed](#)]
48. Kuo, D.-Y.; Eom, C.J.; Kawasaki, J.K.; Petretto, G.; Nelson, J.N.; Hautier, G.; Crumlin, E.J.; Shen, K.M.; Schlom, D.G.; Suntivich, J. Influence of Strain on the Surface—Oxygen Interaction and the Oxygen Evolution Reaction of SrIrO₃. *J. Phys. Chem. C* **2018**, *122*, 4359–4364. [[CrossRef](#)]
49. Stoerzinger, K.A.; Choi, W.S.; Jeen, H.; Lee, H.N.; Shao-Horn, Y. Role of Strain and Conductivity in Oxygen Electrocatalysis on LaCoO₃ Thin Films. *J. Phys. Chem. Lett.* **2015**, *6*, 487–492. [[CrossRef](#)]
50. Tong, Y.; Guo, Y.; Chen, P.; Liu, H.; Zhang, M.; Zhang, L.; Yan, W.; Chu, W.; Wu, C.; Xie, Y. Spin-State Regulation of Perovskite Cobaltite to Realize Enhanced Oxygen Evolution Activity. *Chem* **2017**, *3*, 812–821. [[CrossRef](#)]
51. Petrie, J.R.; Mitra, C.; Jeen, H.; Choi, W.S.; Meyer, T.L.; Reboredo, F.A.; Freeland, J.W.; Eres, G.; Lee, H.N. Strain Control of Oxygen Vacancies in Epitaxial Strontium Cobaltite Films. *Adv. Funct. Mater.* **2016**, *26*, 1564–1570. [[CrossRef](#)]
52. Liu, X.; Zhang, L.; Zheng, Y.; Guo, Z.; Zhu, Y.; Chen, H.; Li, F.; Liu, P.; Yu, B.; Wang, X.; et al. Uncovering the Effect of Lattice Strain and Oxygen Deficiency on Electrocatalytic Activity of Perovskite Cobaltite Thin Films. *Adv. Sci.* **2019**, *6*, 1801898. [[CrossRef](#)]
53. Jung, J.-I.; Risch, M.; Park, S.; Kim, M.G.; Nam, G.; Jeong, H.-Y.; Shao-Horn, Y.; Cho, J. Optimizing nanoparticle perovskite for bifunctional oxygen electrocatalysis. *Energy Environ. Sci.* **2016**, *9*, 176–183. [[CrossRef](#)]
54. Zhou, S.; Miao, X.; Zhao, X.; Ma, C.; Qiu, Y.; Hu, Z.; Zhao, J.; Shi, L.; Zeng, J. Engineering electrocatalytic activity in nanosized perovskite cobaltite through surface spin-state transition. *Nat. Commun.* **2016**, *7*, 1–7. [[CrossRef](#)] [[PubMed](#)]
55. Zhang, L.; Zhu, H.; Hao, J.; Wang, C.; Wen, Y.; Li, H.; Lu, S.; Duan, F.; Du, M. Integrating the cationic engineering and hollow structure engineering into perovskites oxides for efficient and stable electrocatalytic oxygen evolution. *Electrochim. Acta* **2019**, *327*, 135033. [[CrossRef](#)]
56. Zhang, X.; Gong, Y.; Li, S.; Sun, C. Porous Perovskite La_{0.6}Sr_{0.4}Co_{0.8}Mn_{0.2}O₃ Nanofibers Loaded with RuO₂ Nanosheets as an Efficient and Durable Bifunctional Catalyst for Rechargeable Li-O₂ Batteries. *ACS Catal.* **2017**, *7*, 7737–7747. [[CrossRef](#)]
57. Hua, B.; Li, M.; Zhang, Y.-Q.; Sun, Y.-F.; Luo, J.-L. All-In-One Perovskite Catalyst: Smart Controls of Architecture and Composition toward Enhanced Oxygen/Hydrogen Evolution Reactions. *Adv. Energy Mater.* **2017**, *7*, 1700666. [[CrossRef](#)]
58. Zhu, Y.; Zhou, W.; Zhong, Y.; Bu, Y.; Chen, X.; Zhong, Q.; Liu, M.; Shao, Z. A perovskite nanorod as bifunctional electrocatalyst for overall water splitting. *Adv. Energy Mater.* **2017**, *7*, 1602122. [[CrossRef](#)]
59. Xu, J.-J.; Xu, D.; Wang, Z.-L.; Wang, H.-G.; Zhang, L.-L.; Zhang, X.-B. Synthesis of Perovskite-Based Porous La_{0.75}Sr_{0.25}MnO₃ Nanotubes as a Highly Efficient Electrocatalyst for Rechargeable Lithium–Oxygen Batteries. *Angew. Chem. Int. Ed.* **2013**, *52*, 3887–3890. [[CrossRef](#)]
60. Yang, Y.; Yin, W.; Wu, S.; Yang, X.; Xia, W.; Shen, Y.; Huang, Y.; Cao, A.; Yuan, Q. Perovskite-Type LaSrMnO Electrocatalyst with Uniform Porous Structure for an Efficient Li-O₂ Battery Cathode. *ACS Nano* **2016**, *10*, 1240–1248. [[CrossRef](#)]
61. Jin, C.; Cao, X.; Zhang, L.; Zhang, C.; Yang, R. Preparation and electrochemical properties of urchin-like La_{0.8}Sr_{0.2}MnO₃ perovskite oxide as a bifunctional catalyst for oxygen reduction and oxygen evolution reaction. *J. Power Sources* **2013**, *241*, 225–230. [[CrossRef](#)]
62. Yu, H.; Chu, F.; Zhou, X.; Ji, J.; Liu, Y.; Bu, Y.; Kong, Y.; Tao, Y.; Li, Y.; Qin, Y. A perovskite oxide with a tunable pore-size derived from a general salt-template strategy as a highly efficient electrocatalyst for the oxygen evolution reaction. *Chem. Commun.* **2019**, *55*, 2445–2448. [[CrossRef](#)]
63. Li, Z.; Li, J.-G.; Ao, X.; Sun, H.; Wang, H.; Yuen, M.-F.; Wang, C. Conductive metal—Organic frameworks endow high-efficient oxygen evolution of La_{0.6}Sr_{0.4}Co_{0.8}Fe_{0.2}O₃ perovskite oxide nanofibers. *Electrochim. Acta* **2020**, *334*, 135638. [[CrossRef](#)]

64. Wang, Y.; Wang, Z.; Jin, C.; Li, C.; Li, X.; Li, Y.; Yang, R.; Liu, M. Enhanced overall water electrolysis on a bifunctional perovskite oxide through interfacial engineering. *Electrochim. Acta* **2019**, *318*, 120–129. [\[CrossRef\]](#)
65. Gao, Y.; Wang, J.; Lyu, Y.-Q.; Lam, K.; Ciucci, F. In situ growth of Pt 3 Ni nanoparticles on an A-site deficient perovskite with enhanced activity for the oxygen reduction reaction. *J. Mater. Chem. A* **2017**, *5*, 6399–6404. [\[CrossRef\]](#)
66. Gao, Y.; Lu, Z.; You, T.L.; Wang, J.; Xie, L.; He, J.; Ciucci, F. Energetics of Nanoparticle Exsolution from Perovskite Oxides. *J. Phys. Chem. Lett.* **2018**, *9*, 3772–3778. [\[CrossRef\]](#) [\[PubMed\]](#)
67. Lindenthal, L.; Rameshan, R.; Summerer, H.; Ruh, T.; Popovic, J.; Nenning, A.; Löffler, S.; Opitz, A.K.; Blaha, P.; Rameshan, C. Modifying the Surface Structure of Perovskite-Based Catalysts by Nanoparticle Exsolution. *Catalysts* **2020**, *10*, 268. [\[CrossRef\]](#)
68. Neagu, D.; Tsekouras, G.; Miller, D.N.; Ménard, H.; Irvine, J.T. In situ growth of nanoparticles through control of non-stoichiometry. *Nat. Chem.* **2013**, *5*, 916–923. [\[CrossRef\]](#)
69. Ji, D.; Cai, S.; Paudel, T.R.; Sun, H.; Zhang, C.; Han, L.; Wei, Y.; Zang, Y.; Gu, M.; Zhang, Y.; et al. Freestanding crystalline oxide perovskites down to the monolayer limit. *Nature* **2019**, *570*, 87–90. [\[CrossRef\]](#)
70. Zhao, H.; Chen, C.; Chen, D.; Saccoccio, M.; Wang, J.; Gao, Y.; Wan, T.H.; Ciucci, F. Ba_{0.95}La_{0.05}FeO_{3-δ}-multi-layer graphene as a low-cost and synergistic catalyst for oxygen evolution reaction. *Carbon* **2015**, *90*, 122–129. [\[CrossRef\]](#)
71. Xu, Y.; Tsou, A.; Fu, Y.; Wang, J.; Tian, J.-H.; Yang, R. Carbon-Coated Perovskite BaMnO₃ Porous Nanorods with Enhanced Electrocatalytic Performance for Oxygen Reduction and Oxygen Evolution. *Electrochim. Acta* **2015**, *174*, 551–556. [\[CrossRef\]](#)
72. Wang, J.; Zhao, H.; Gao, Y.; Chen, D.; Chen, C.; Saccoccio, M.; Ciucci, F. Ba_{0.5}Sr_{0.5}Co_{0.8}Fe_{0.2}O_{3-δ} on N-doped mesoporous carbon derived from organic waste as a bi-functional oxygen catalyst. *Int. J. Hydrog. Energy* **2016**, *41*, 10744–10754. [\[CrossRef\]](#)
73. Wang, J.; Gao, Y.; Ciucci, F. Mechanochemical Coupling of MoS₂ and Perovskites for Hydrogen Generation. *ACS Appl. Energy Mater.* **2018**, *1*, 6409–6416. [\[CrossRef\]](#)
74. Oh, N.K.; Kim, C.; Lee, J.; Kwon, O.; Choi, Y.; Jung, G.Y.; Lim, H.Y.; Kwak, S.K.; Kim, G.; Park, H. In-situ local phase-transitioned MoSe₂ in La_{0.5}Sr_{0.5}CoO_{3-δ} heterostructure and stable overall water electrolysis over 1000 hours. *Nat. Commun.* **2019**, *10*, 1723. [\[CrossRef\]](#)
75. Fabbri, E.; Nachtegaal, M.; Cheng, X.; Schmidt, T.J. Superior Bifunctional Electrocatalytic Activity of Ba_{0.5}Sr_{0.5}Co_{0.8}Fe_{0.2}O_{3-δ}/Carbon Composite Electrodes: Insight into the Local Electronic Structure. *Adv. Energy Mater.* **2015**, *5*, 1402033. [\[CrossRef\]](#)
76. Zhang, Z.; Wang, J.; Chen, Y.; Tan, S.; Shao, Z.; Chen, D. In situ formation of a 3D core-shell and triple-conducting oxygen reduction reaction electrode for proton-conducting SOFCs. *J. Power Sources* **2018**, *385*, 76–83. [\[CrossRef\]](#)
77. Zhang, H.-M.; Teraoka, Y.; Yamazoe, N. Preparation of perovskite-type oxides with large surface area by citrate process. *Chem. Lett.* **1987**, *16*, 665–668. [\[CrossRef\]](#)
78. Bu, Y.; Jang, H.; Gwon, O.; Kim, S.H.; Joo, S.H.; Nam, G.; Kim, S.; Qin, Y.; Zhong, Q.; Kwak, S.K. Synergistic interaction of perovskite oxides and N-doped graphene in versatile electrocatalyst. *J. Mater. Chem. A* **2019**, *7*, 2048–2054. [\[CrossRef\]](#)
79. Guan, D.; Zhou, J.; Huang, Y.-C.; Dong, C.-L.; Wang, J.-Q.; Zhou, W.; Shao, Z. Screening highly active perovskites for hydrogen-evolving reaction via unifying ionic electronegativity descriptor. *Nat. Commun.* **2019**, *10*, 3755. [\[CrossRef\]](#)
80. Dai, J.; Zhu, Y.; Zhong, Y.; Miao, J.; Lin, B.; Zhou, W.; Shao, Z. Enabling High and Stable Electrocatalytic Activity of Iron-Based Perovskite Oxides for Water Splitting by Combined Bulk Doping and Morphology Designing. *Adv. Mater. Interfaces* **2019**, *6*, 1801317. [\[CrossRef\]](#)
81. Hona, R.K.; Ramezanipour, F. Remarkable Oxygen-Evolution Activity of a Perovskite Oxide from the Ca_{2-x}Sr_xFe₂O_{6-δ} Series. *Angew. Chem. Int. Ed.* **2019**, *58*, 2060–2063. [\[CrossRef\]](#)
82. Zhao, B.; Zhang, L.; Zhen, D.; Yoo, S.; Ding, Y.; Chen, D.; Chen, Y.; Zhang, Q.; Doyle, B.; Xiong, X.; et al. A tailored double perovskite nanofiber catalyst enables ultrafast oxygen evolution. *Nat. Commun.* **2017**, *8*, 14586. [\[CrossRef\]](#)

83. Suntivich, J.; May, K.J.; Gasteiger, H.A.; Goodenough, J.B.; Shao-Horn, Y. A perovskite oxide optimized for oxygen evolution catalysis from molecular orbital principles. *Science* **2011**, *334*, 1383–1385. [\[CrossRef\]](#) [\[PubMed\]](#)
84. May, K.J.; Carlton, C.E.; Stoerzinger, K.A.; Risch, M.; Suntivich, J.; Lee, Y.-L.; Grimaud, A.; Shao-Horn, Y. Influence of oxygen evolution during water oxidation on the surface of perovskite oxide catalysts. *J. Phys. Chem. Lett.* **2012**, *3*, 3264–3270. [\[CrossRef\]](#)
85. Jung, J.-I.; Park, S.; Kim, M.-G.; Cho, J. Tunable Internal and Surface Structures of the Bifunctional Oxygen Perovskite Catalysts. *Adv. Energy Mater.* **2015**, *5*, 1501560. [\[CrossRef\]](#)
86. Ou, G.; Yang, C.; Liang, Y.; Hussain, N.; Ge, B.; Huang, K.; Xu, Y.; Wei, H.; Zhang, R.; Wu, H. Surface Engineering of Perovskite Oxide for Bifunctional Oxygen Electrocatalysis. *Small Methods* **2019**, *3*, 1800279. [\[CrossRef\]](#)
87. Zhang, C.; Berlinguette, C.P.; Trudel, S. Water oxidation catalysis: An amorphous quaternary Ba-Sr-Co-Fe oxide as a promising electrocatalyst for the oxygen-evolution reaction. *Chem. Commun.* **2016**, *52*, 1513–1516. [\[CrossRef\]](#)
88. Grimaud, A.; Diaz-Morales, O.; Han, B.; Hong, W.T.; Lee, Y.-L.; Giordano, L.; Stoerzinger, K.A.; Koper, M.T.; Shao-Horn, Y. Activating lattice oxygen redox reactions in metal oxides to catalyse oxygen evolution. *Nat. Chem.* **2017**, *9*, 457. [\[CrossRef\]](#)
89. Wang, H.; Wang, J.; Pi, Y.; Shao, Q.; Tan, Y.; Huang, X. Double Perovskite LaFe_xNi_{1-x}O₃ nanorods enable efficient oxygen evolution electrocatalysis. *Angew. Chem.* **2019**, *131*, 2338–2342. [\[CrossRef\]](#)
90. Zhang, D.; Song, Y.; Du, Z.; Wang, L.; Li, Y.; Goodenough, J.B. Active LaNi_{1-x}Fe_xO₃ bifunctional catalysts for air cathodes in alkaline media. *J. Mater. Chem. A* **2015**, *3*, 9421–9426. [\[CrossRef\]](#)
91. Höfer, H.E.; Schmidberger, R. Electronic Conductivity in the La(Cr, Ni)O₃ Perovskite System. *J. Electrochem. Soc.* **1994**, *141*, 782–786. [\[CrossRef\]](#)
92. Bockris, J.O.M.; Otagawa, T. The electrocatalysis of oxygen evolution on perovskites. *J. Electrochem. Soc.* **1984**, *131*, 290. [\[CrossRef\]](#)
93. Jung, S.; McCrory, C.C.; Ferrer, I.M.; Peters, J.C.; Jaramillo, T.F. Benchmarking nanoparticulate metal oxide electrocatalysts for the alkaline water oxidation reaction. *J. Mater. Chem. A* **2016**, *4*, 3068–3076. [\[CrossRef\]](#)
94. Wang, J.; Ciucci, F. Boosting Bifunctional Oxygen Electrolysis for N-Doped Carbon via Bimetal Addition. *Small* **2017**, *13*, 1604103. [\[CrossRef\]](#) [\[PubMed\]](#)
95. Forslund, R.P.; Hardin, W.G.; Rong, X.; Abakumov, A.M.; Filimonov, D.; Alexander, C.T.; Mefford, J.T.; Iyer, H.; Kolpak, A.M.; Johnston, K.P.; et al. Exceptional electrocatalytic oxygen evolution via tunable charge transfer interactions in La_{0.5}Sr_{1.5}Ni_{1-x}Fe_xO_{4±δ} Ruddlesden-Popper oxides. *Nat. Commun.* **2018**, *9*, 3150. [\[CrossRef\]](#)
96. Petrie, J.R.; Cooper, V.R.; Freeland, J.W.; Meyer, T.L.; Zhang, Z.; Lutterman, D.A.; Lee, H.N. Enhanced Bifunctional Oxygen Catalysis in Strained LaNiO₃ Perovskites. *J. Am. Chem. Soc.* **2016**, *138*, 2488–2491. [\[CrossRef\]](#) [\[PubMed\]](#)
97. Retuerto, M.; Pereira, A.G.; Pérez-Alonso, F.J.; Peña, M.A.; Fierro, J.L.G.; Alonso, J.A.; Fernández-Díaz, M.T.; Pascual, L.; Rojas, S. Structural effects of LaNiO₃ as electrocatalyst for the oxygen reduction reaction. *Appl. Catal. B Environ.* **2017**, *203*, 363–371. [\[CrossRef\]](#)
98. Bak, J.; Bin Bae, H.; Chung, S.-Y. Atomic-scale perturbation of oxygen octahedra via surface ion exchange in perovskite nickelates boosts water oxidation. *Nat. Commun.* **2019**, *10*, 2713. [\[CrossRef\]](#)
99. Lee, J.G.; Hwang, J.; Hwang, H.J.; Jeon, O.S.; Jang, J.; Kwon, O.; Lee, Y.; Han, B.; Shul, Y.-G. A new family of perovskite catalysts for oxygen-evolution reaction in alkaline media: BaNiO₃ and BaNi_{0.83}O_{2.5}. *J. Am. Chem. Soc.* **2016**, *138*, 3541–3547. [\[CrossRef\]](#)
100. Zhang, J.; Cui, Y.; Jia, L.; He, B.; Zhang, K.; Zhao, L. Engineering anion defect in LaFeO_{2.85}Cl_{0.15} perovskite for boosting oxygen evolution reaction. *Int. J. Hydrog. Energy* **2019**, *44*, 24077–24085. [\[CrossRef\]](#)
101. Xu, X.; Chen, Y.; Zhou, W.; Zhong, Y.; Guan, D.; Shao, Z. Earth-Abundant Silicon for Facilitating Water Oxidation over Iron-Based Perovskite Electrocatalyst. *Adv. Mater. Interfaces* **2018**, *5*, 1701693. [\[CrossRef\]](#)
102. Zhu, K.; Liu, H.; Li, X.; Li, Q.; Wang, J.; Zhu, X.; Yang, W. Oxygen evolution reaction over Fe site of BaZr_xFe_{1-x}O_{3-δ} perovskite oxides. *Electrochim. Acta* **2017**, *241*, 433–439. [\[CrossRef\]](#)
103. Shen, Z.; Zhuang, Y.; Li, W.; Huang, X.; Oropeza, F.E.; Hensen, E.J.M.; Hofmann, J.P.; Cui, M.; Tadich, A.; Qi, D.; et al. Increased activity in the oxygen evolution reaction by Fe⁴⁺-induced hole states in perovskite La_{1-x}Sr_xFeO₃. *J. Mater. Chem. A* **2020**, *8*, 4407–4415. [\[CrossRef\]](#)

104. Najafpour, M.M. Calcium-manganese oxides as structural and functional models for active site in oxygen evolving complex in photosystem II: Lessons from simple models. *J. Photochem. Photobiol. B Biol.* **2011**, *104*, 111–117. [[CrossRef](#)] [[PubMed](#)]
105. Gagrani, A.; Alsultan, M.; Swiegers, G.F.; Tsuzuki, T. Comparative evaluation of the structural and other features governing photo-electrochemical oxygen evolution by Ca/Mn oxides. *Catal. Sci. Technol.* **2020**, *10*, 2152–2164. [[CrossRef](#)]
106. Yamada, I.; Fujii, H.; Takamatsu, A.; Ikeno, H.; Wada, K.; Tsukasaki, H.; Kawaguchi, S.; Mori, S.; Yagi, S. Bifunctional Oxygen Reaction Catalysis of Quadruple Manganese Perovskites. *Adv. Mater.* **2017**, *29*, 1603004. [[CrossRef](#)]
107. Chen, D.; Wang, J.; Zhang, Z.; Shao, Z.; Ciucci, F. Boosting oxygen reduction/evolution reaction activities with layered perovskite catalysts. *Chem. Commun.* **2016**, *52*, 10739–10742. [[CrossRef](#)]
108. Miao, H.; Wang, Z.; Wang, Q.; Sun, S.; Xue, Y.; Wang, F.; Zhao, J.; Liu, Z.; Yuan, J. A new family of Mn-based perovskite ($\text{La}_{1-x}\text{Y}_x\text{MnO}_3$) with improved oxygen electrocatalytic activity for metal-air batteries. *Energy* **2018**, *154*, 561–570. [[CrossRef](#)]
109. Yamada, I.; Takamatsu, A.; Asai, K.; Ohzuku, H.; Shirakawa, T.; Uchimura, T.; Kawaguchi, S.; Tsukasaki, H.; Mori, S.; Wada, K.; et al. Synergistically Enhanced Oxygen Evolution Reaction Catalysis for Multielement Transition-Metal Oxides. *ACS Appl. Energy Mater.* **2018**, *1*, 3711–3721. [[CrossRef](#)]
110. Yoo, J.S.; Rong, X.; Liu, Y.; Kolpak, A.M. Role of lattice oxygen participation in understanding trends in the oxygen evolution reaction on perovskites. *ACS Catal.* **2018**, *8*, 4628–4636. [[CrossRef](#)]
111. Zhang, L.; Raman, A.S.; Vojvodic, A. Reviving Inert Oxides for Electrochemical Water Splitting by Subsurface Engineering. *Chem. Mater.* **2020**. [[CrossRef](#)]
112. Kushwaha, H.S.; Halder, A.; Thomas, P.; Vaish, R. $\text{CaCu}_3\text{Ti}_4\text{O}_{12}$: A Bifunctional Perovskite Electrocatalyst for Oxygen Evolution and Reduction Reaction in Alkaline Medium. *Electrochim. Acta* **2017**, *252*, 532–540. [[CrossRef](#)]
113. Yamada, I.; Takamatsu, A.; Asai, K.; Shirakawa, T.; Ohzuku, H.; Seno, A.; Uchimura, T.; Fujii, H.; Kawaguchi, S.; Wada, K.; et al. Systematic Study of Descriptors for Oxygen Evolution Reaction Catalysis in Perovskite Oxides. *J. Phys. Chem. C* **2018**, *122*, 27885–27892. [[CrossRef](#)]
114. Chen, C.-F.; King, G.; Dickerson, R.M.; Papin, P.A.; Gupta, S.; Kellogg, W.R.; Wu, G. Oxygen-deficient BaTiO_{3-x} perovskite as an efficient bifunctional oxygen electrocatalyst. *Nano Energy* **2015**, *13*, 423–432. [[CrossRef](#)]
115. Tymińska, N.; Wu, G.; Dupuis, M. Water oxidation on oxygen-deficient barium titanate: A first-principles study. *J. Phys. Chem. C* **2017**, *121*, 8378–8389. [[CrossRef](#)]
116. Artrith, N.; Sailuam, W.; Limpijumnong, S.; Kolpak, A.M. Reduced overpotentials for electrocatalytic water splitting over Fe- and Ni-modified BaTiO_3 . *Phys. Chem. Chem. Phys.* **2016**, *18*, 29561–29570. [[CrossRef](#)] [[PubMed](#)]

